JOURNAL OF GEOPHYSICAL RESEARCH, VOL. 105, NO. B2, PAGES 2981-3000, FEBRUARY 10, 2000

Equivalent medium representation of fractured rock

Enru Liu
British Geological Survey, Edinburgh, Scotland, United Kingdom

John A. Hudson
Department of Applied Mathematics and Theoretical Physics, University of Cambridge
Cambridge, England, United Kingdom

Tim Pointer
BG plc., Gas Research and Technology Centre, Loughborough, England, United Kingdom

Abstract. A similarity may be found between various approaches for determining the effects of parallel fractures or aligned cracks on seismic wave propagation at wavelengths that are long compared with the scale length of the cracks. Fractures can be modeled using an empirical linear slip condition; however, natural fracture surfaces can also be simulated directly as planar distributions of small isolated areas of slip (cracks) (model 1) or, conversely, as planar distributions of imperfect interfacial contacts (model 2). An alternative is plane surfaces separated by thin continuous layers of viscous fluid or a soft material (model 3). We present analytic expressions for the fracture compliances for these three models and, using these analytic results, compute the effective compliances and stiffnesses of the fractured material. As a result, it is possible to relate the measured compliances or stiffnesses directly to the statistics of the microstructural details of a fracture, given appropriate a priori information on the fracture surfaces. The results for model 1 are equivalent to a volume distribution of cracks as studied by *Hudson* [1980, 1981] for small crack density; the results for model 2 are basically the same as those given by *White* [1983] for a packing of spheres; and finally, the results for model 3 are in agreement with those given by *Backus* [1962] for combinations of two constituent layers. These results can be extended to the case of nonaligned fractures and to allow for fluid flow between cracks and into a porous matrix rock. Finally, it is shown that the ratio of the normal to shear fracture compliance is a good indicator of the properties of the fracture infill.

1. Introduction

Fractures and faults are common in the subsurface of the Earth's crust, and they control much of the mechanical strength and transport properties of the solid structure. Fractures and fracture systems are also crucial for hydrocarbon production, control and manipulation of water supplies, and dispersal of pollutants. Much of our knowledge about the Earth's crust is obtained from seismic waves. One of the most successful methods for the detection and characterization of fractures and the prediction of fluid flow directions is the use of seismic shear waves [*Queen and Rizer*, 1990]. *Queen et al.* [1992] argue that fractures may be common in the crust but that only a few open fractures may control the fluid flow; they also emphasize that stress controls fracture distributions and thus fluid flow pathways. Figure 1 shows the relationship between fracture patterns and associated stress fields [after *Cosgrove*, 1998]. *Crampin and Atkinson* [1985] suggest that the fracture patterns of the type in Figure 1a may be common in the crust except in near-surface structures where fractures may have more complex patterns.

There have been many theories in the literature that attempt to predict effective properties of a rock mass containing distributed cracks (reviewed by *Hudson and Knopoff* [1989]). Recently, *Sayers and Kachanov* [1995], and *Schoenberg and Sayers* [1995] have presented a new formalism for calculating the effective elastic constants for cracked and fractured media. Both models are based on *Hill*'s [1963] concept of average stress and strain [*Hudson and Knopoff*, 1989] and assume a linear relationship governed by the fracture compliance $\boldsymbol{Z}$, between displacement discontinuity across fractures and the applied tractions. *Sayers and Kachanov* [1995] define two tensors (a second-rank tensor and a fourth-rank

Paper number 1999JB900306.
0148-0227/00/1999JB900306$09.00

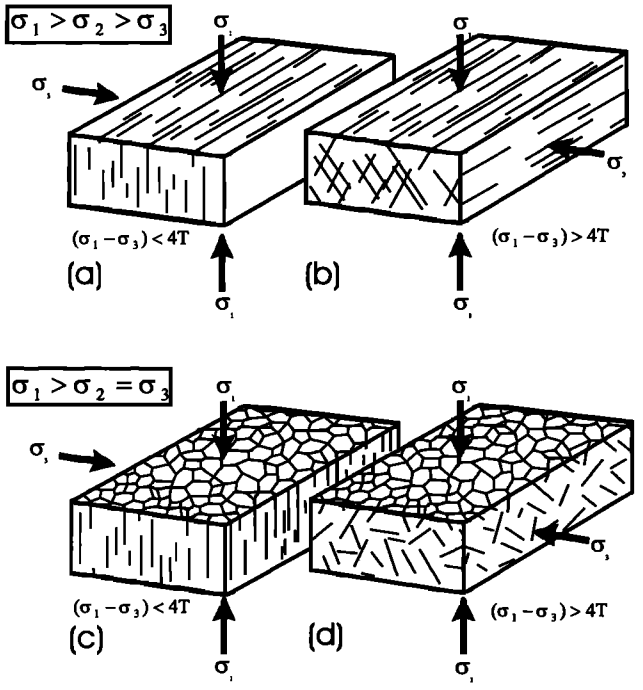

Figure 1. Three-dimensional patterns of fractures: (a) when $\sigma_1 - \sigma_3 < 4T$ and the two horizontal principal stresses are unequal; (b) when $\sigma_1 - \sigma_3 > 4T$ and the two horizontal principal stresses are unequal; (c) when $\sigma_1 - \sigma_3 < 4T$ and $\sigma_2 = \sigma_3$; and (d) when $\sigma_1 - \sigma_3 > 4T$ and $\sigma_2 = \sigma_3$. T is the tensile strength of the rock [after *Cosgrove*, 1998].

tensor) to calculate the overall wave properties; both are related to the fracture compliance. *Schoenberg and Sayers* [1995] use laboratory measurements and *Hudson*'s [1981] results to estimate the fracture compliance parameters. On the basis of this work they conclude that it is not possible to distinguish between microcracks and macrofractures.

In this paper we shall present a model in which *Hudson et al.*'s [1996b, 1997] boundary conditions are used to compute the fracture compliance $\boldsymbol{Z}$ directly, and these are then used to calculate the effective elastic compliance of fractured rock using formulae similar to those in *Sayers and Kachanov* [1995], and *Schoenberg and Sayers* [1995]. The purposes of this paper are twofold: first, to show that several different fracture models can be cast into a unified form, and second, to show that the fracture compliance tensor $\boldsymbol{Z}$, can be related to the microstructure of the fractures. We consider fractures modeled as (1) a planar distribution of small, isolated areas of slip (cracks); (2) a planar distribution of isolated interfacial contacts (welds); and (3) an idealized open fracture with weak infill material. Models 1 and 2 are derived from the belief that natural fracture surfaces may be simulated by groups of small crack-like features. Contact between two nonconforming surfaces goes through several phases as the driving pressure increases [*Nagy*, 1992]. In the earlier stages, when the pressure driving the surfaces is low, contact consists of isolated areas (kissing contact) with the remaining surface areas being separated. This is represented by model 2. As the pressure increases, the contact areas grow and join up until, in the later stages, only some isolated areas remain out of contact. This is represented by model 1. This process is idealized by representing the areas of contact in model 2 and the separated areas in model 1 as circular. Such simplification is not absolutely necessary since whatever the shape of crack or weld, a numerical solution can be constructed for its elastic response. However, the result would not be as simple or transparent as the analytic expressions obtained for circular cracks or welds. In the end, however, it is impossible to create a model with exactly the same geometry as a real fracture. Nor does anyone want or need such details. What is looked for are the statistics of the fracture surface - number density of cracks or welds, their average diameter, and so forth. The basic assumption of models of this kind is that the mechanical response of a fracture with a complex structure will be approximately the same as a fracture with circular cracks or welds with the same crack statistics. If this is so, the values of the crack statistics inferred from data using an idealized theory based on circular cracks will be a quantitative measure of the statistics of the actual fracture. Models 1 and 2 are, of course, quite different in character, and there will be fractures with a microstructure which is not realistically represented by either. Model 3 is one that has been around for a long time and provides a format into which the results for models 1 and 2 fit. It represents the state of a fracture before the driving pressure induces areas of contact between the fracture faces. At this point, model 2 takes over.

The smoothed boundary conditions for models 1 and 2 were obtained recently by *Hudson et al.* [1996b, 1997] and are similar in form to the empirical formulae of *Murty* [1976] and *Pyrak-Nolte et al.* [1990]. The main advantage of the method presented in this paper is that unlike the earlier empirical models of fractures, all parameters involved have physical meaning (subject to the assumptions referred to above), and fracture compliances are shown to be directly related to the details of the microstructure of the fracture planes.

In this paper we shall refer to a crack as the small compact area of cohesion loss on a fracture surface, whose size is very much smaller than a wavelength, and to a fracture as the larger-scale fluid flow system, whose size is still much smaller than the seismic wavelength. A fault is made up of many fractures, and we model the fault region as a random distribution of fractures. Whereas cracked material has, in general, been modeled as a random distribution of cracks, the fault region studied here under model 1 has the cracks confined to the fracture surfaces. In this way the cracks appear as clusters, and the difference in the formulae for the two cases can be interpreted as the effect of one form

of clustering. Under model 3 we are back to a random distribution of cracks (we call them fractures here to differentiate between these and the microcracks on a fracture surface in model 1) but with the possibility of any kind of infill. Model 2 is similar to model 3 except that the fracture stiffness is increased by areas of contact (welds). It is novel in the sense that the open region on the fracture is extensive and complex.

2. Fracture Models

In modeling the seismic response of natural and induced fractures it is essential to understand the microscopic details of fractures as fluid flow is controlled by microstructures of fracture or fault planes [*Jones and Knipe*, 1996]. Intensive studies have addressed this problem because of its conceptual and practical importance. The general understanding is that a fracture is a cluster of small cracks, and a fault is a cluster of fractures. Cracks often exist as clusters at different scales, as schematically shown in Figure 2. Several fracture models have been proposed in geophysics, acoustics, and nondestructive testing in studies of the mechanical, transport, and seismic properties of fractures. *Newmark et al.* [1951] and *Jones and Whittier* [1967] were among the earliest attempts to study an "incomplete" interface (fracture), for which averaged boundary conditions relating tractions and displacements were derived. (Such a model is also called unbonded, loosely bonded, unwelded, nonwelded, imperfect, unperfect, or a slip interface by various authors in the literature.) *Murty* [1976] considered a vanishingly thin layer of viscous fluid which leads to boundary conditions similar to those of *Newmark et al.* [1951]; he also gave numerical results for the reflected and transmitted energy for incident plane waves. The transmission and reflection properties of seismic waves across a thin layer of viscous fluid were studied by *Fehler* [1982] specifically to interpret acoustic events induced by hydraulic fracturing. The effect of a thin weak elastic layer was more recently investigated by *Rokhlin and Wang* [1991]. *Schoenberg* [1980], *Myer et al.* [1990], *Pyrak-Nolte et al.* [1990], and *Nihei et al.* [1994] extended *Murty's* [1976] model and assumed that the discontinuity in each component of displacement is proportional to the corresponding component of traction. Further generality was introduced by *Tleukenov* [1991], who considered thin layers filled with anisotropic elastic or linearly viscoelastic material and also derived a nonlinear relationship between displacement discontinuity and traction. *Angel and Achenbach* [1985] studied the problem of elastic wave diffraction by interface imperfections due to periodic arrays of cracks. The displacement discontinuity and traction relationship for a random planar distribution of microcracks and for a similar distribution of welded areas in an otherwise unbonded interface were derived by *Hudson et al.* [1996b, 1997] and discussed by *Liu et al.* [1996]; the former is similar to the rough surface fracture model of *Gangi* [1981]. Note that *Kozlov* [1997] uses the results published by *Liu et al.* [1996] to study the effective elastic properties and transmission and reflection characteristics of fractured rock.

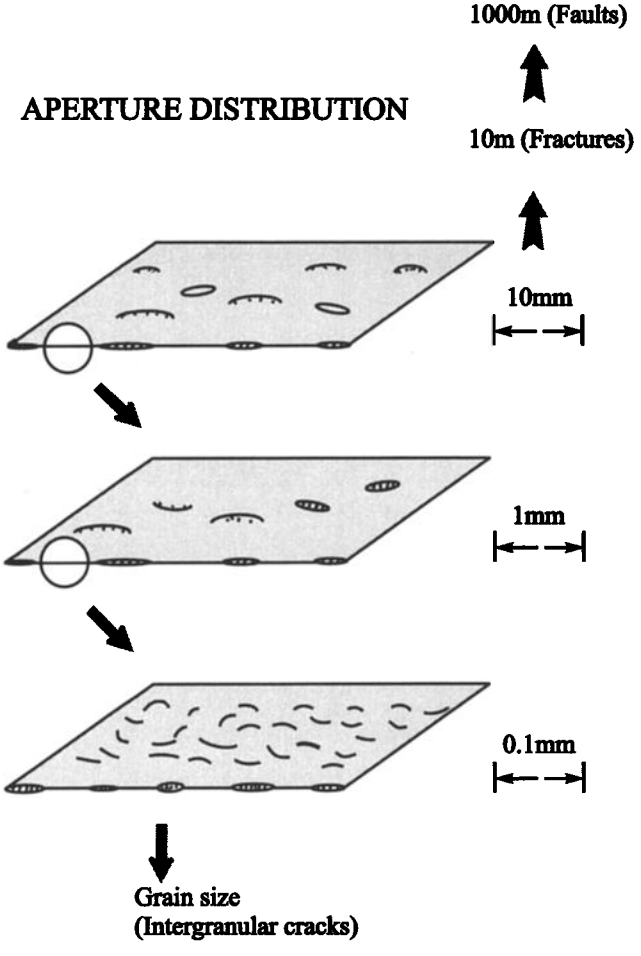

Figure 2. Schematic illustration of the distribution of cracks at different scales. (Courtesy of Bill Rizer, formerly at Conoco Inc.).

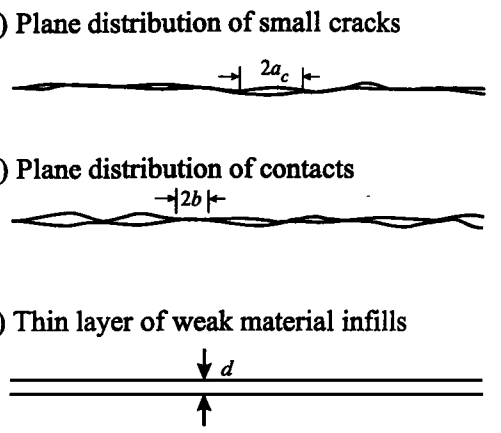

Figure 3. Schematic illustration of three fracture models. (a) A plane distribution of small cracks; (b) a plane distribution of contacts, and (c) a thin layer of weak solid material with a constant aperture.

In summary, published fracture models can be broadly classified into three groups, which are schematically shown in Figure 3. Model 1 (Figure 3a) portrays a plane distribution of small cracks and model 2 (Figure 3b) portrays a plane distribution of contacts. Both models can be replaced with an equivalent fracture of constant aperture with appropriate material infill (model 3, Figure 3c) as demonstrated by *Hudson and Liu* [1999].

3. Effective Compliance of a Solid Containing Parallel Fractures

We begin by considering a system of parallel plane fractures. Each fracture has a structure in accordance with one of models 1, 2, or 3. In the presence of fractures the average strain $\boldsymbol{\epsilon}$ in an elastic homogeneous solid with volume V containing N_f fractures with surfaces S_r ($r = 1, 2, ..., N_f$) can be written as

$$\epsilon_{ij} = (s^0_{ijkl} + s^f_{ijkl})\sigma_{kl}, \tag{1}$$

where $\boldsymbol{\sigma}$ is the average stress tensor, $\boldsymbol{s}^0$ is the matrix compliance tensor in the absence of the fractures, and $\boldsymbol{s}^f$ is the extra compliance tensor resulting from the fractures. The additional strain is given by [*Hill*, 1963 and *Hudson and Knopoff*, 1989]

$$s^f_{ijkl}\sigma_{kl} = \frac{1}{2V}\sum_{r=1}^{N_f}\int_{S_r}\left([u_i]n_j + [u_j]n_i\right)dS, \tag{2}$$

where $[u_i]$ is the ith component of the displacement discontinuity on S_r and n_i is the ith component of the fracture normal. If all fractures are aligned with fixed normal $\boldsymbol{n}$, we may replace each fracture in V by an average fracture having a surface area S and a smoothed linear slip boundary condition given by

$$[\overline{u}_i] = Z_{ip}t_p, \tag{3}$$

where $\boldsymbol{t}$ is the traction on the fracture, $[\overline{u}_i]$ is the average displacement discontinuity on the fracture, and the quantities $\{Z_{ij}\}$ depend on the interior conditions and infill of the fracture (*Schoenberg and Sayers* [1995], *Sayers and Kachanov* [1995]). The traction t_p is linearly related to the imposed mean stress $\boldsymbol{\sigma}$ or, more precisely, to the traction $\sigma_{pq}n_q$ which would exist on the crack face if the displacements were constrained to be zero. We use a model of a simple fracture in an unbounded medium (Appendix A) and write

$$t_p = T_{pq}\sigma_{qs}n_s, \tag{4}$$

where the elements $\{T_{pq}\}$ depend on the $\{Z_{ij}\}$. Equation (3) becomes

$$[\overline{u}_i] = Z_{ip}T_{pq}\sigma_{qs}n_s. \tag{5}$$

Inserting (5) into (2), we obtain, after some tensor algebra,

$$\begin{aligned} s^f_{ijkl}\sigma_{kl} &= \frac{N_f S}{4V}\left(Z_{ip}T_{pk}n_l n_j + Z_{jp}T_{pk}n_l n_i\right. \\ &+ \left. Z_{ip}T_{pl}n_k n_j + Z_{jp}T_{pl}n_k n_i\right)\sigma_{kl}, \end{aligned} \tag{6}$$

where S is the mean area of a fracture; so the fracture-induced excess compliance s^f_{ijkl} is

$$\begin{aligned} s^f_{ijkl} &= \frac{D_f}{4}\left(Z_{ip}T_{pk}n_l n_j + Z_{jp}T_{pk}n_l n_i\right. \\ &+ \left. Z_{ip}T_{pl}n_k n_j + Z_{jp}T_{pl}n_k n_i\right), \end{aligned} \tag{7}$$

where we have defined D_f to be

$$D_f = \frac{N_f S}{V}. \tag{8}$$

If the fracture set is statistically invariant under rotations about $\boldsymbol{n}$, only two terms in $\boldsymbol{Z}$ are required (*Schoenberg and Sayers* [1995]): a normal fracture compliance Z_N and a tangential compliance Z_T. Thus

$$\begin{aligned} Z_{ij} &= Z_N n_i n_j + Z_T(\delta_{ij} - n_i n_j) \\ &= Z_T\delta_{ij} + (Z_N - Z_T)n_i n_j, \end{aligned} \tag{9}$$

where δ_{ij} is the Kroneker delta. Furthermore, $\boldsymbol{T}$ is also diagonal:

$$T_{ij} = T_N n_i n_j + T_T(\delta_{ij} - n_i n_j). \tag{10}$$

where (see Appendix A)

$$T_N = \left[1 + \frac{3\pi\mu Z_N}{4a_f}\left(\frac{\lambda+\mu}{\lambda+2\mu}\right)\right]^{-1}, \tag{11a}$$

and

$$T_T = \left[1 + \frac{3\pi\mu Z_T}{16a_f}\left(\frac{3\lambda+4\mu}{\lambda+2\mu}\right)\right]^{-1}; \tag{11b}$$

λ, μ are the Lamé constants of the uncracked matrix material and a_f is the average radius of a fracture. By inserting (9) and (11) into (7), we have

$$\begin{aligned} s^f_{ijkl} &= \frac{D_f}{4}\left[Z'_T\left(\delta_{ik}n_l n_j + \delta_{jk}n_l n_i + \delta_{il}n_k n_j\right.\right. \\ &+ \left.\left.\delta_{jl}n_k n_i\right) + 4\left(Z'_N - Z'_T\right)n_i n_j n_k n_l\right], \end{aligned} \tag{12}$$

where $Z'_N = Z_N T_N$ and $Z'_T = Z_T T_T$. This equation is equivalent to equation (9) of *Sayers and Kachanov* [1995] and also equation (9) of *Schoenberg and Sayers* [1995]. To determine the stiffness c_{ijkl}, it is convenient to transform the s_{ijkl} to the conventional (two-subscript) condensed 6 x 6 matrix notation, 11 → 1, 22 → 2, 33 → 3, 23 → 4, 13 → 5, 12 → 6, with factors 2 and 4 introduced as follows: $s_{ijkl} \to s_{pq}$ when both of p, q are 1, 2, or 3; $2s_{ijkl} \to s_{pq}$ when one of p, q is 4, 5, or 6; and $4s_{ijkl} \to s_{pq}$ when both of p, q are 4,

5, or 6. The inverse of the compliance matrix s_{pq} gives the effective elastic constants or stiffness matrix c_{pq} in terms of the two fracture parameters Z'_N and Z'_T. (See *Auld* [1990] or *Nye* [1985] for details).

In order to use (12) to compute effective elastic compliance, *Sayers and Kachanov* [1995] define two tensors, one proportional to Z'_T and the other to $Z'_N - Z'_T$ (a second-rank tensor and a fourth-rank tensor, respectively). *Schoenberg and Sayers* [1995] and *Sayers and Kachanov* [1995] point out that the results are particularly simple if $Z'_N = Z'_T$, in which case the fourth-rank tensor vanishes. In the following sections, we shall consider three fracture models that have been studied by *Hudson et al.* [1996b, 1997] and *Hudson and Liu* [1999], who give explicit expressions for Z_N and Z_T in terms of physical parameters.

4. Model 1: Fracture Modeled as a Planar Distribution of Small Isolated Areas of Slip or Cracks

Following *Hudson et al.* [1996b], where a fracture is modeled as a planar distribution of small isolated areas of slip (cracks) with an average circular shape of radius a_c, the two fracture parameters Z_N and Z_T are given by

$$Z_T = \frac{\gamma_c a_c^3}{\mu} A_T, \qquad Z_N = \frac{\gamma_c a_c^3}{\mu} A_N, \tag{13}$$

where γ_c is the number of elementary cracks per unit area, μ is the shear modulus of the uncracked rock (matrix), and A_T and A_N are given as

$$A_T = U_{11}\Big[1 + (\gamma_c a_c^2)^{3/2} U_{11} \frac{\pi}{4}(3 - 2\beta^2/\alpha^2)\Big], \tag{14a}$$

and

$$A_N = U_{33}\Big[1 + (\gamma_c a_c^2)^{3/2} U_{33} \pi(1 - \beta^2/\alpha^2)\Big], \tag{14b}$$

where $\alpha = [(\lambda + 2\mu)/\rho]^{1/2}$ and $\beta = (\mu/\rho)^{1/2}$ are the P and S wave velocities, respectively, of the uncracked solid, and ρ is the density of the uncracked solid. The parameters U_{11} and U_{33} correspond to the response of a single crack to shear traction and tension, respectively. Expressions for U_{11} and U_{33} for a range of crack models are available in the literature; for example, dry cracks, cracks filled with fluids or weak materials [*Hudson*, 1981], partial saturation [*Hudson*, 1988], and fluid flow between interconnected cracks in porous media [*Hudson et al.*, 1996a; T. Pointer et al., Seismic wave propagation in cracked porous media, submitted to *Geophysical Journal International*, 1999, hereinafter referred to as Pointer et al., submitted manuscript, 1999]. Note that in the result given above, dynamic interactions between cracks on the same fracture plane are taken into account through the second terms in the brackets in (14), but interactions between different fractures are neglected. Note also that equations (14a) and (14b) are valid only for wavelengths that are long compared with the size of the fractures.

Inserting (11), (13), and (14) into (12), we obtain the following for fracture-induced excess compliance:

$$\begin{aligned} s^f_{ijkl} &= \frac{\varepsilon}{4\mu}\big[A'_T(\delta_{ik}n_l n_j + \delta_{jk}n_l n_i + \delta_{il}n_k n_j \\ &+ \delta_{jl}n_k n_i) + 4(A'_N - A'_T)n_i n_j n_k n_l\big], \end{aligned} \tag{15}$$

where

$$A'_N = A_N\left[1 + \frac{3\pi}{4}\frac{\gamma_c a_c^3}{a_f} A_N\Big(\frac{\lambda + \mu}{\lambda + 2\mu}\Big)\right]^{-1}, \tag{16a}$$

and

$$A'_T = A_T\left[1 + \frac{3\pi}{16}\frac{\gamma_c a_c^3}{a_f} A_T\Big(\frac{3\lambda + 4\mu}{\lambda + 2\mu}\Big)\right]^{-1}, \tag{16b}$$

and we have written

$$\varepsilon = D_f \gamma_c a_c^3 \equiv \frac{N_f S}{V}\frac{N_c a_c^3}{S} \equiv \frac{N a_c^3}{V}, \tag{17}$$

which is called the crack density; by definition, $\gamma_c = N_c/S$ is the average number of cracks N_c on a fracture surface of area S, and the total number of elementary cracks N in the volume V is $N = N_f N_c$. (N_f is the number of fractures defined in (2).) The parameter D_f ($=N_f S/V$) has the dimensions of inverse length; if the fractures were infinite parallel planes, D_f would correspond to H_f^{-1}, where H_f is the mean spacing between the fracture planes. The quantity V/N is the average volume per unit crack. If we write $V/N = l^3$, l is roughly the average spacing between cracks. Similarly, by writing $S/N_c = (\gamma_c)^{-1} = l_c^2$, l_c is approximately a mean distance between cracks on a fracture. We characterize the fractures as a clustering of cracks, so we expect that $l_c < l$. From (17) we see that $D_f^{-1} = H_f = l^3/l_c^2$, and so we expect $H_f > l$ in general; H_f is, in fact, a measure of the clustering of cracks onto fractures.

To the first order in the number densities ε and $\varepsilon_c = \gamma_c a_c^2$, (16) become $A'_T = U_{11}$ and $A'_N = U_{33}$, respectively. By inverting (15), we obtain the following expressions for the elastic stiffnesses written in conventional (two-subscript) condensed 6 x 6 matrix notations and assuming $\boldsymbol{n} = (1, 0, 0)$:

$$c_{11} = (\lambda + 2\mu)\Big(1 + \frac{\lambda + 2\mu}{\mu}\varepsilon U_{33}\Big)^{-1}, \tag{18a}$$

$$\begin{aligned} c_{22} &= c_{33} = \Big[(\lambda + 2\mu) + 4(\lambda + \mu)\varepsilon U_{33}\Big] \\ &\Big(1 + \frac{\lambda + 2\mu}{\mu}\varepsilon U_{33}\Big)^{-1}, \end{aligned} \tag{18b}$$

$$c_{12} = c_{13} = c_{21} = c_{31} = \lambda\Big(1 + \frac{\lambda + 2\mu}{\mu}\varepsilon U_{33}\Big)^{-1}, \quad (18c)$$

$$c_{23} = c_{32} = \lambda(1 + 2\varepsilon U_{33})\Big(1 + \frac{\lambda + 2\mu}{\mu}\varepsilon U_{33}\Big)^{-1}, \quad (18d)$$

$$c_{55} = c_{66} = \mu\Big(1 + \varepsilon U_{11}\Big)^{-1}, \quad (18e)$$

and $c_{44} = (c_{22} - c_{23})/2 = \mu$; all other terms are zero. If we define

$$E_T = \varepsilon U_{11}, \qquad E_N = \frac{\lambda + 2\mu}{\mu}\varepsilon U_{33}, \quad (19)$$

equation (18) is equivalent to those given by *Schoenberg and Douma* [1988]. For comparison, *Hudson*'s [1981] first-order expressions for a volume distribution of cracks whose normals point in the $\boldsymbol{n} = (1, 0, 0)$ direction may be written as

$$c_{11} = (\lambda + 2\mu)\Big(1 - \frac{\lambda + 2\mu}{\mu}\varepsilon U_{33}\Big), \quad (20a)$$

$$c_{22} = c_{33} = \Big[(\lambda + 2\mu) + 4(\lambda + \mu)\varepsilon U_{33}\Big]\Big(1 - \frac{\lambda + 2\mu}{\mu}\varepsilon U_{33}\Big), \quad (20b)$$

$$c_{12} = c_{13} = c_{21} = c_{31} = \lambda\Big(1 - \frac{\lambda + 2\mu}{\mu}\varepsilon U_{33}\Big), \quad (20c)$$

$$c_{23} = c_{32} = \lambda(1 + 2\varepsilon U_{33})\Big(1 - \frac{\lambda + 2\mu}{\mu}\varepsilon U_{33}\Big), \quad (20d)$$

$$c_{55} = c_{66} = \mu\Big(1 - \varepsilon U_{11}\Big), \quad (20e)$$

and $c_{44} = (c_{22} - c_{23})/2 = \mu$; all other terms are zero. We can immediately find that (18) reduce to (20) if ε is sufficiently small; that is, if

$$\Big(1 - \frac{\lambda + 2\mu}{\mu}\varepsilon U_{33}\Big) \simeq \Big(1 + \frac{\lambda + 2\mu}{\mu}\varepsilon U_{33}\Big)^{-1}, \quad (21)$$

and if

$$\Big(1 - \varepsilon U_{11}\Big) \simeq \Big(1 + \varepsilon U_{11}\Big)^{-1}. \quad (22)$$

These approximations will be reasonable if the following inequalities are satisfied:

$$\frac{\lambda + 2\mu}{\mu}\varepsilon U_{33} \ll 1, \qquad \varepsilon U_{11} \ll 1. \quad (23)$$

If we assume that the matrix is a Poisson solid and use expressions for U_{11} and U_{33} for dry cracks (given below), this requirement becomes $\varepsilon \ll \frac{f}{6} \simeq 0.17$. In these circumstances, (18) or (20) constitute the standard first-order result for a distribution of cracks. The clustering of cracks on the faults is nowhere reflected in these formulae. To assess the effect of clustering, we need to go to higher-order terms.

If we include the higher-order terms in crack density, the terms U_{11} and U_{33} in (18) should be replaced with A'_T and A'_N given in (14) and (16).

For dry cracks, *Hudson* [1981] gives

$$U_{11} = U_{11}^d = \frac{16}{3}\frac{\lambda + 2\mu}{3\lambda + 4\mu} = \frac{16}{3}\frac{1 - \nu}{2 - \nu}, \quad (24a)$$

and

$$U_{33} = U_{33}^d = \frac{4}{3}\frac{\lambda + 2\mu}{\lambda + \mu} = \frac{8}{3}(1 - \nu), \quad (24b)$$

where ν is Poisson's ratio for the uncracked solid: $\nu = \lambda/[2(\lambda + \mu)]$. It follows that by inserting (24) into (13) and (14) we have

$$\frac{A'_N}{A'_T} \simeq \frac{Z_N}{Z_T} = \frac{1}{4}\frac{3\lambda + 4\mu}{\lambda + \mu} = 1 - \frac{\nu}{2} \quad (25)$$

to first-order in the number density. This result was used by *Schoenberg and Sayers* [1995] and *Sayers and Kachanov* [1995] to justify dropping the last term in the brackets in (15) for $\boldsymbol{s}^f$ (as ν is usually small and typically in the range $0.1 \le \nu \le 0.25$). Note that for water-filled cracks, *Hudson* [1981] obtained $U_{33} \simeq 0$ and $U_{11} = U_{11}^d$ provided aspect ratio of cracks is very small, and in this case, we have $A'_N/A'_T = Z_N/Z_T = 0$.

Figure 4 compares the variation of elastic parameters c_{11} and c_{66} (normalized by the equivalent parameters of the uncracked solid) with crack density ε, using *Hudson*'s [1980, 1981] theory up to second-order in crack density and the theory for model 1 above (also including higher-order terms). The variations are calculated for a solid with background wave speeds $\alpha = 3300$ m/s, $\beta = 1800$ m/s, and density $\rho = 2.2$ g/cm^3 (the material properties are appropriate for sandstone [see *Batzle and Wang*, 1992]) and the cracks are filled with water with acoustic velocity of $\alpha_f = 1500$ m/s and density of $\rho_f = 1.0$ g/cm^3 (Figure 4a) and air (gas or dry) (Figure 4b). The cracks have an average aspect ratio of 0.01 and $a_c/H_f = 0.5$ and $a_c/a_f = 0.1$. *Hudson*'s [1981] results as indicated by solid lines are very close to the results of this paper for crack densities of up to 0.1 for cracks filled with both water and air (Figure 4a) and with air (Figure 4b). Beyond the limit of 0.15 for the air-filled cracks, the normalized stiffness continues to decrease for the new model, but the results from *Hudson* [1981] show a systematic and unphysical increase. We would not expect complete correspondence between the two theories even though they both include crack-crack interactions. The results given in this paper correspond to a concentration of cracks onto fractures so that while interactions between cracks on the same fracture are included, those between different fractures are ignored.

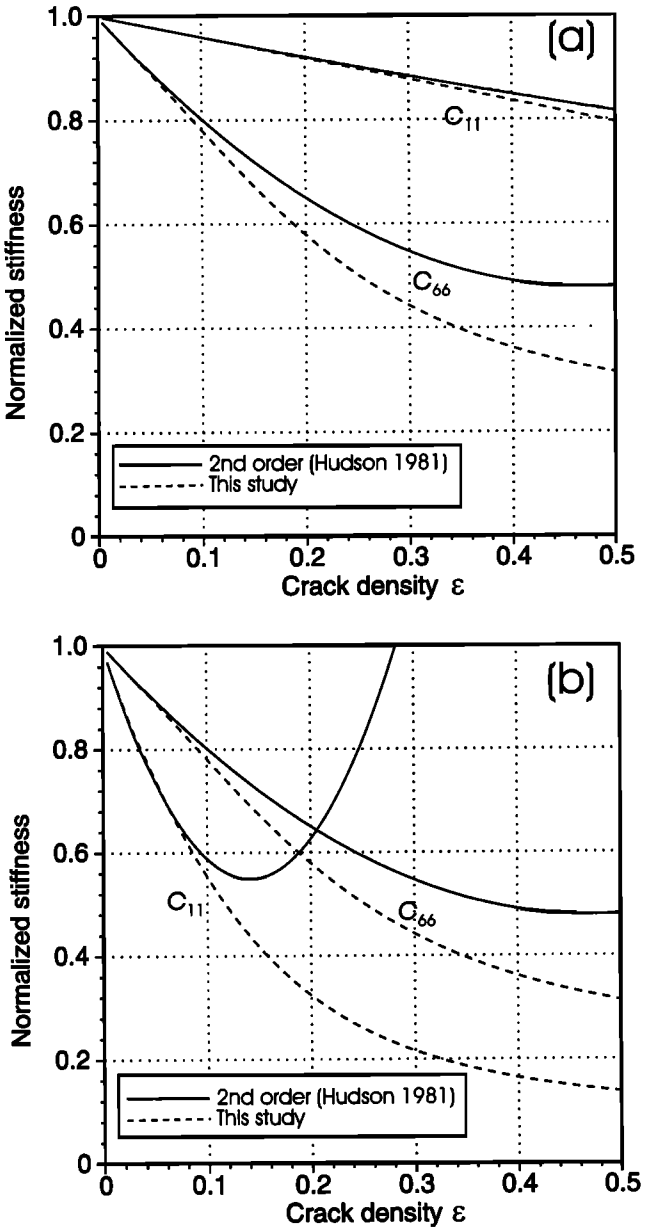

Figure 4. Variations of normalized elastic constants c_{11} and c_{66} against crack density ε. Two theories which include crack-crack interactions are compared: *Hudson's* [1981] volume distribution of small cracks and a distribution of fractures with each surface modeled as a planar distribution of small cracks (studied in this paper): (a) water-filled cracks and (b) dry cracks. For the solid matrix, $\alpha = 3300$ m/s, $\beta = 1800$ m/s, and $\rho = 2.2$ g/cm^3, and for the water, $\alpha_f = 1500$ m/s and $\rho_f = 1.0$ g/cm^3. The cracks have an average aspect ratio of 0.01, $a_c/a_f = 0.1$ and $a_c/H_f = 0.5$.

Figure 5 compares the variation with crack density of the two normalized stiffnesses c_{11} and c_{66} computed from various theories: the differential effective medium (DEM) theory of *Nishizawa* [1982], *Hudson's* [1980, 1981] first-order and second-order models, and the results of the present study. Again the variations are calculated for both water (Figures 5a and 5b) and gas-filled cracks (Figures 5c and 5d). All parameters are the same as those used in Figure 4. We see that the results from this study are close to the DEM results for crack densities up to 0.5. This demonstrates another feature of current theory; by working in terms of compliances rather than stiffnesses, we have results which appear physically reasonable at crack densities much greater than the expected range of validity of the theory. This is in contrast to *Hudson's* [1980, 1981] earlier result, which, when ε grows beyond the range in which the approximations are strictly valid, gives results which are not physically realistic, as can be seen in Figure 4. The question as to whether the current results (or the DEM values) are correct for the idealized models that we have used at relatively high values of ε can only be resolved by numerical experiment.

Figures 6a and 6b show the variations of the normalized elastic constants c_{11} and c_{66} with crack density for four different values of $D_f a_c$ $(= a_c/H_f)$ as indicated in Figures 6a and 6b. The cracks are filled with water with all parameters are the same as those used in Figure 4 except $a_c/a_f = 0.0001$. The quantity a_c/H_f is equal to $\varepsilon/\varepsilon_c$, or $a_c l_c^2/l^3$, where l_c is the spacing of cracks on a fracture and l is the mean overall spacing of the cracks. It follows that decreasing values of a_c/H_f correspond to increasing in level of clustering of cracks on a fault. The variations of elastic stiffnesses with crack density show a strong dependence on the value of a_c/H_f. This shows clearly the effect of clustering of cracks onto faults.

5. Model 2: Fracture Modeled as a Planar Distribution of Imperfect Facial Contacts or Rough Surface

In contrast to the fracture model described above, a fracture can also be simulated as a planar distribution of imperfect interfacial contacts (partial bond, known also as a kissing bond). This model has been studied in the past by several authors [e.g., *Stoll*, 1989, *White*, 1983, *Yoshioka*, 1994, *Xu and King*, 1992]. Similar interface conditions to (3) have been obtained for a dry (empty) fracture [*Hudson et al.*, 1997], and to second-order in number density of contacts, we have

$$Z_T = \frac{1}{\gamma_w \mu b} B_T, \qquad Z_N = \frac{1}{\gamma_w \mu b} B_N, \tag{26}$$

where

$$B_T = \frac{3\lambda + 4\mu}{8(\lambda + \mu)} \left[1 + 2(\gamma_w b^2)^{1/2}\right]^{-1}, \tag{27a}$$

and

$$B_N = \frac{\lambda + 2\mu}{4(\lambda + \mu)} \left[1 + 2(\gamma_w b^2)^{1/2}\right]^{-1}, \tag{27b}$$

where γ_w is the number density of contacts (i.e., the ratio of the number of contacts N_w on a surface to its

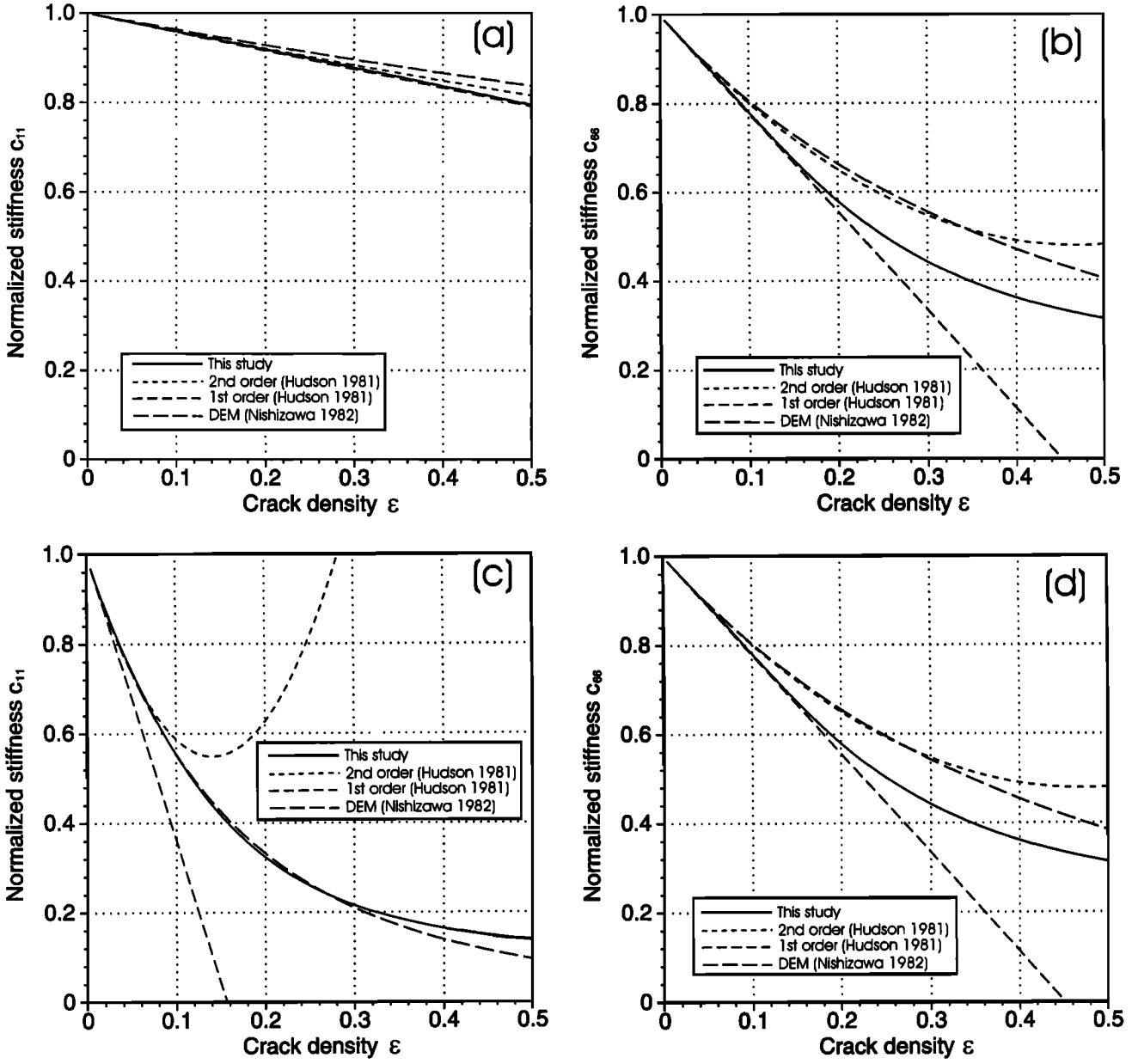

Figure 5. Comparison of normalized elastic constants calculated using various theories for crack density up to 0.5 (water-filled cracks only): (a) and (b) for water-filled cracks and (c) and (d) for dry or gas-filled cracks. Elastic parameters are as for Figure 4.

area S; $\gamma_w = N_w/S$); b is the average radius of welded regions (contacts). These equations are valid if $\gamma_w b^2$ is small. Inserting (26) and (27) into (12), we obtain

$$s^f_{ijkl} = \frac{\varepsilon_f}{4\mu}\Big[B'_T\Big(\delta_{ik}n_l n_j + \delta_{jk}n_l n_i + \delta_{il}n_k n_j + \delta_{jl}n_k n_i\Big) + 4(B'_N - B'_T)n_i n_j n_k n_l\Big], \quad (28)$$

where

$$B'_N = U^d_{33}\Big[1 + \frac{4}{3\pi}\frac{\gamma_w a_f b}{B_N}\Big(\frac{\lambda+2\mu}{\lambda+\mu}\Big)\Big]^{-1}, \quad (29a)$$

and

$$B'_T = U^d_{11}\Big[1 + \frac{16}{3\pi}\frac{\gamma_w a_f b}{B_T}\Big(\frac{\lambda+2\mu}{3\lambda+4\mu}\Big)\Big]^{-1}, \quad (29b)$$

and we have written

$$\varepsilon_f = \frac{D_f a_f}{\pi} = \frac{N_f S}{V}\frac{a_f}{\pi} = \frac{N_f}{V}a_f^3, \quad (30)$$

which may be called the fracture density (note that $S = \pi a_f^2$).

For a vanishingly small density of contacts ($\varepsilon_w = \gamma_w b^2 \ll 1$) we have

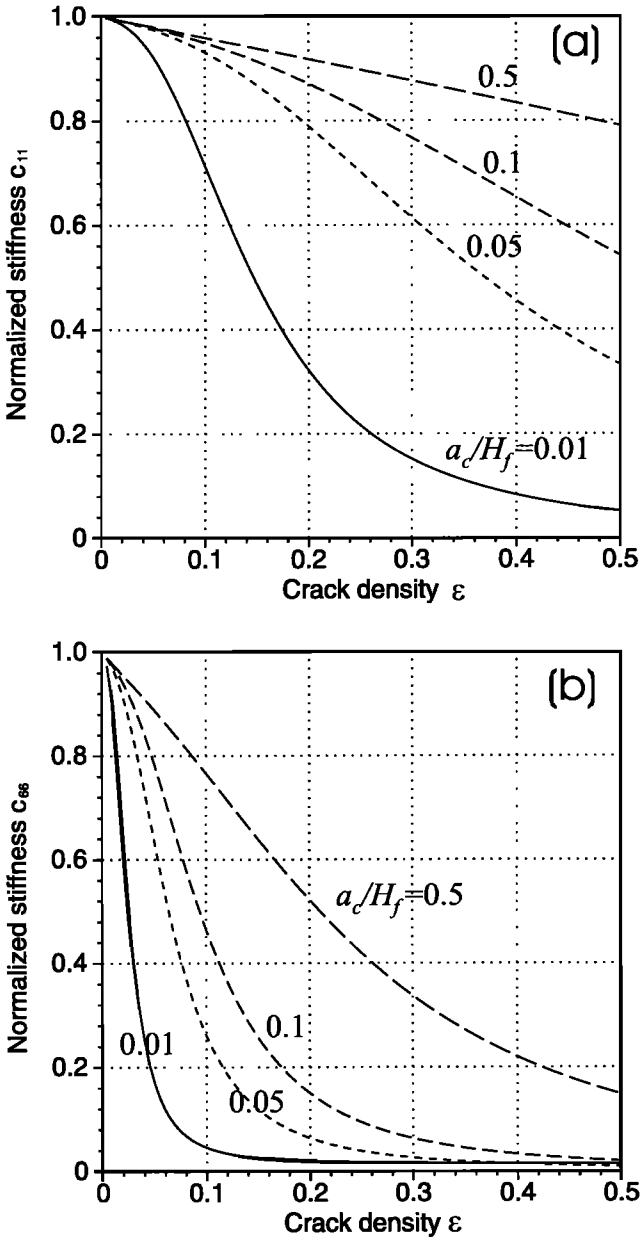

Figure 6. Variation of (a) normalized c_{11} and (b) c_{66} with crack density. For comparison, the solid line is calculated from a volume distribution of small cracks [*Hudson*, 1981] and the dashed lines are from plane distributions of small cracks (this paper) for three different values of D_f $(= a_c/H_f)$. Other parameters are as for Figure 4 except $a_c/a_f = 0.0001$.

$$B'_N = U^d_{33}, \qquad B'_T = U^d_{11}, \tag{31a}$$

and the fractures become like dry cracks of radius a_f as expected. This may be contrasted with Section 4, where we saw that for low crack density on the fractures $(\gamma_c a_c^2 \ll 1)$ the material responds as with a random distribution of noninteracting cracks of radius a_c. If b/a_f is very small, we obtain

$$B'_N = B_N, \qquad B'_T = B_T. \tag{31b}$$

The elastic stiffness in 2-index notation can be derived as before (assuming $\boldsymbol{n} = (1, 0, 0)$):

$$c_{11} = (\lambda + 2\mu)\Big(1 + \frac{\lambda + 2\mu}{\mu}\varepsilon_f B'_N\Big)^{-1}, \tag{32a}$$

$$c_{22} = c_{33} = \Big[(\lambda + 2\mu) + 4(\lambda + \mu)\varepsilon_f B'_N\Big]\Big(1 + \frac{\lambda + 2\mu}{\mu}\varepsilon_f B'_N\Big)^{-1}, \tag{32b}$$

$$c_{12} = c_{13} = c_{21} = c_{31} = \lambda\Big(1 + \frac{\lambda + 2\mu}{\mu}\varepsilon_f B'_N\Big)^{-1}, \tag{32c}$$

$$c_{23} = c_{32} = \lambda(1 + 2\varepsilon_f B'_N)\Big(1 + \frac{\lambda + 2\mu}{\mu}\varepsilon_f B'_N\Big)^{-1}, \tag{32d}$$

$$c_{55} = c_{66} = \mu\Big(1 + \varepsilon_f B'_T\Big)^{-1}, \tag{32e}$$

and $c_{44} = (c_{22} - c_{23})/2 = \mu$; all other terms are zero.

Note that from (29) we have

$$\frac{B'_N}{B'_T} = \Big(\frac{1}{4}\frac{3\lambda + 4\mu}{\lambda + \mu}\Big)M_1 \tag{33a}$$

where

$$M_1 = \left\{\frac{1 + \frac{16}{3\pi}\gamma_w a_f b \frac{8(\lambda+\mu)(\lambda+2\mu)}{(3\lambda+4\mu)^2}[1 + 2(\gamma_w b^2)^{1/2}]}{1 + \frac{16}{3\pi}\gamma_w a_f b[1 + 2(\gamma_w b^2)^{1/2}]}\right\},$$

which for a Poisson solid is approximately 7/8, once again leading to the conclusion that the last term on the right of (28) may be regarded as small.

If b/a_f is small, we have $B'_N = B_N$ and $B'_T = B_T$. In this case, B'_N and B'_T in (32) can be replaced with B_N and B_T, respectively. If $\gamma^w b^2$ is also small, the second terms in the brackets in (27) may be ignored, and we have

$$\frac{B'_N}{B'_T} \simeq \frac{B_N}{B_T} \simeq \frac{2(\lambda + 2\mu)}{3\lambda + 4\mu} = \frac{1 - \nu}{1 - \nu/2}, \tag{33b}$$

which agrees with the result of *White* [1983], and equation (33b) is cited by *Sayers and Kachanov* [1995] to justify their assumption of $Z_N = Z_T$.

Figures 7a and 7b show the variations of normalized elastic constants c_{11} and c_{66} for parallel dry fractures with a plane distribution of small contacts. The variations are plotted against fracture density ε_f and for five different values of the parameter, $r = 1 - \gamma_w \pi b^2$, and r can be regarded as the proportion of the fault

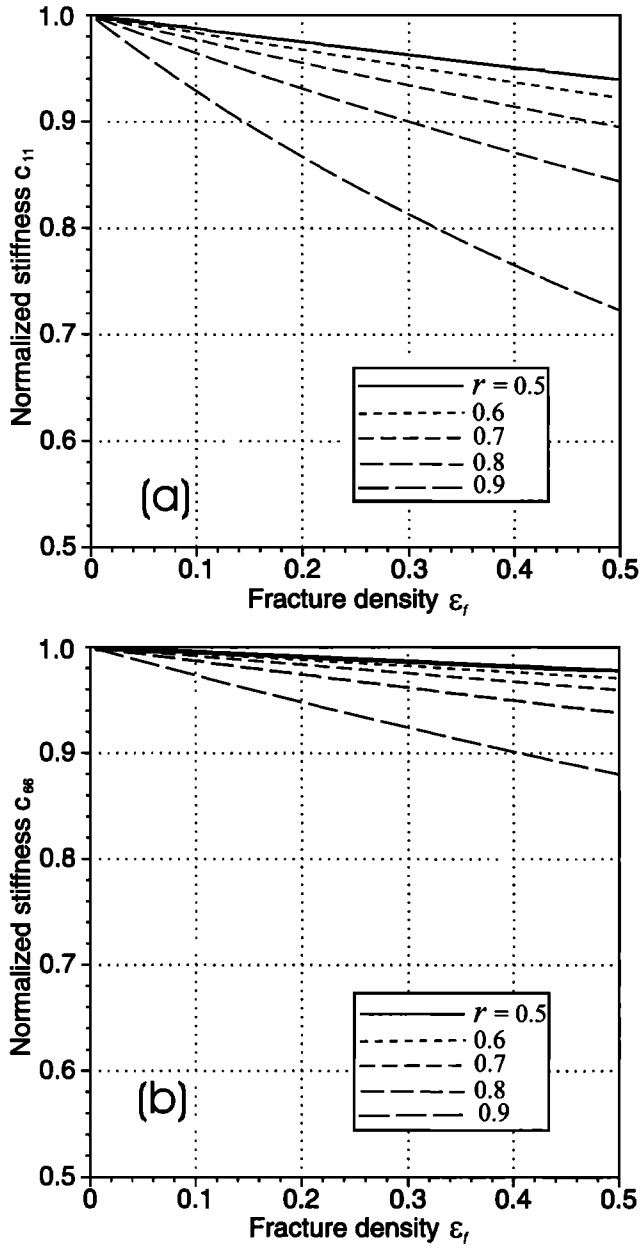

Figure 7. Variation of (a) normalized c_{11} and (b) c_{66} with fracture density ε_f computed for various values of the parameter $r = 1 - \gamma_w \pi b^2$; γ_w is the number density of welded regions on unit area of fracture surface, and b is the averaged radius of a welded area. Other parameters are as for Figure 4 except $b/a_f = 0.01$.

face that consists of open cracks. The results are only valid for small $\gamma_w \pi b^2$, so we assume $0.5 \leq r \leq 1$. All other parameters are the same as those used in Figure 4 except $b/a_f = 0.01$. The values of normalized c_{11} and c_{66} decrease as ε_f increases and are strongly dependent on the value $r = 1 - \gamma_w \pi b^2$.

Note that (26) and (27) are valid for dry fractures, and for liquid-filled fractures, B_T remains unchanged, and $B_N = 0$ [*Hudson and Liu*, 1999], so we have $B'_N/B'_T = 0$.

Unfortunately, the theory formulated above does not allow for the cracked regions in this model to be filled with any material other than air (dry cracks) or an inviscid incompressible fluid. One way of avoiding this difficulty is discussed by *Hudson and Liu* [1999].

6. Model 3: Fracture Modeled as a Thin, Continuous Layer Filled With a Weak Solid

The third fracture model is a continuous, parallel-walled layer filled with a weak solid. This model is often used to represent hydraulic fractures [e.g., *Fehler*, 1982, *Groenenboom and Fokkema*, 1998, *Meadows and Winterstein*, 1994, *Liu et al.*, 1997]. Using the method presented in Appendix B, it is possible to derive the following expressions:

$$Z_T = \frac{d}{\mu} C_T, \qquad Z_N = \frac{d}{\mu} C_N, \tag{34}$$

where C_T and C_N are given by (from equation (B9))

$$C_T = \frac{\mu}{\mu_f + i\omega\eta_f}, \tag{35a}$$

$$C_N = \frac{\mu}{\lambda_f + 2\mu_f + \frac{4}{3} i\omega\eta_f}, \tag{35b}$$

respectively; λ_f and μ_f are the Lamé constants, η_f is the viscosity of the fracture infill material, d is the average fracture aperture (assumed to be much smaller than a wavelength), and ω is frequency. Inserting (34) and (35) into (12), the fracture-induced excess compliance can be obtained:

$$\begin{aligned} s^f_{ijkl} &= \frac{\varepsilon_f}{4\mu}\Big[C'_T\Big(\delta_{ik}n_l n_j + \delta_{jk}n_l n_i + \delta_{il}n_k n_j \\ &+ \delta_{jl}n_k n_i\Big) + 4\Big(C'_N - C'_T\Big)n_i n_j n_k n_l\Big], \end{aligned} \tag{36}$$

where

$$C'_N = U^d_{33}\Big[1 + \frac{4}{3\pi}\frac{a_f}{dC_N}\Big(\frac{\lambda + 2\mu}{\lambda + \mu}\Big)\Big]^{-1}, \tag{37a}$$

$$C'_T = U^d_{11}\Big[1 + \frac{16}{3\pi}\frac{a_f}{dC_T}\Big(\frac{\lambda + 2\mu}{3\lambda + 4\mu}\Big)\Big]^{-1}, \tag{37b}$$

and ε_f is defined as before (equation (30)). The effective elastic stiffness can once again be obtained by inversion of effective elastic compliance and in condensed matrix form, and we have, exactly, the same equations as (32) except that B'_N and B'_T are replaced by C'_N and C'_T, respectively. Alternatively, we may write

$$s^f_{ijkl} = \frac{\phi}{4\mu}\Big[C''_T\Big(\delta_{ik}n_ln_j + \delta_{jk}n_ln_i + \delta_{il}n_kn_j + \delta_{jl}n_kn_i\Big) + 4\Big(C''_N - C''_T\Big)n_in_jn_kn_l\Big], \quad (38)$$

where

$$C''_N = C_N\Big[1 + \frac{3\pi d}{4a_f}C_N\Big(\frac{\lambda+\mu}{\lambda+2\mu}\Big)\Big]^{-1}, \quad (39a)$$

and

$$C''_T = C_T\Big[1 + \frac{3\pi d}{16a_f}C_T\Big(\frac{3\lambda+4\mu}{\lambda+2\mu}\Big)\Big]^{-1}, \quad (39b)$$

and we have defined

$$\phi = dD_f = \frac{N_f S d}{V}, \quad (40)$$

as the porosity of the fractured material.

If we neglect the second terms in the brackets in (39) (assuming (d/a_f) is small), we have $C''_N = C_N$ and $C''_T = C_T$. In this case, the stiffnesses are given by

$$c_{11} = (\lambda+2\mu)\Big(1 + \frac{\lambda+2\mu}{\mu}\phi C_N\Big)^{-1} = \Big[\frac{1}{\lambda+2\mu} + \frac{\phi}{\lambda_f+2\mu_f+\frac{4}{3}i\omega\eta_f}\Big]^{-1}, \quad (41a)$$

$$c_{22} = c_{33} = \Big[(\lambda+2\mu) + 4(\lambda+\mu)\phi C_N\Big]\Big(1 + \frac{\lambda+2\mu}{\mu}\phi C_N\Big)^{-1}, \quad (41b)$$

$$c_{12} = c_{13} = c_{21} = c_{31} = \lambda\Big(1 + \frac{\lambda+2\mu}{\mu}\phi C_N\Big)^{-1}, \quad (41c)$$

$$c_{23} = c_{32} = \lambda(1+2\phi C_N)\Big(1 + \frac{\lambda+2\mu}{\mu}\phi C_N\Big)^{-1}, \quad (41d)$$

$$c_{55} = c_{66} = \mu\Big(1+\phi C_T\Big)^{-1} = \Big[\frac{1}{\mu} + \frac{\phi}{\mu_f+i\omega\eta_f}\Big]^{-1}, \quad (41e)$$

and $c_{44} = (c_{22} - c_{23})/2 = \mu$; all other terms are zero. The expressions for c_{11} and $c_{55} = c_{66}$ can be compared with those given by *Backus* [1962] and *Schoenberg and Muir* [1989] for combinations of two constituent layers

$$c_{11} = \Big[\frac{1-\phi}{\lambda+2\mu} + \frac{\phi}{\lambda_f+2\mu_f+\frac{4}{3}i\omega\eta_f}\Big]^{-1}, \quad (41a')$$

and

$$c_{55} = c_{66} = \Big[\frac{1-\phi}{\mu} + \frac{\phi}{\mu_f+i\omega\eta_f}\Big]^{-1}. \quad (41e')$$

The expressions for other terms are less obvious but can be made similar to *Backus'* [1962] average by systematically ignoring the higher-order terms in porosity ϕ (noting that λ_f and μ_f are usually much smaller than λ and μ). When ϕ is small, (41a') and (41e') are expected to give results very similar to (41a) and (41e).

If fracture is dry, both Z_N and Z_T tend to infinity as λ_f and μ_f go to zero, and in this case, the compliances are as for dry cracks, the same result as for model 2 when the number of density of contacts goes to zero. On the other hand, if the fracture is filled with liquid, Z_N is usually much smaller than Z_T, as κ_f $(= \lambda_f + 2/3\mu_f)$ is much larger than μ_f, which can usually be assumed to be zero. In general, if the fracture is filled with a weak solid, we have from (37)

$$\frac{Z_N}{Z_T} \simeq \frac{C''_N}{C''_T} = \frac{C'_N}{C'_T} = \frac{1}{4}\Big(\frac{3\lambda+4\mu}{\lambda+\mu}\Big)M_2, \quad (42a)$$

where

$$M_2 = \left\{\frac{1 + \frac{16}{3\pi}\frac{a_f}{d}\Big(\frac{\mu_f+i\omega\eta_f}{\mu}\Big)\Big(\frac{\lambda+2\mu}{3\lambda+4\mu}\Big)}{1 + \frac{4}{3\pi}\frac{a_f}{d}\Big(\frac{\lambda_f+2\mu_f+\frac{4}{3}i\omega\eta_f}{\mu}\Big)\Big(\frac{\lambda+2\mu}{\lambda+\mu}\Big)}\right\},$$

which reduces to (25) when fractures are dry ($\lambda_f = \mu_f = 0$).

If d/a_f is small, we have from (39) $C''_N = C_N$ and $C''_T = C_T$ (assuming $\omega\eta_f/\mu$ is also small)

$$\frac{C''_N}{C''_T} = \frac{C_N}{C_T} = \frac{\mu_f}{\lambda_f+2\mu_f} = \Big(\frac{\beta_f}{\alpha_f}\Big)^2, \quad (42b)$$

where α_f and β_f are the P and S wave velocities of the fracture infill. Clearly, for water-filled fracture, $C_N/C_T = 0$.

Figures 8a and 8b show the variations of normalized elastic constants c_{11} and c_{66} for model 3. The variations are plotted against fracture density ε_f and for five different values of the parameter d/a_f. The results are only valid for small d/a_f, so we assume $\leq d/a_f \leq 0.1$. The values of normalized c_{11} and c_{66} decrease as ε_f increases and are strongly dependent on the value d/a_f.

It is worth pointing out that the boundary conditions for models 1 and 2 can be put into a form similar to (34) and (35), so that these two models can be replaced with equivalent layers with appropriate thickness and bulk and shear moduli for the crack infill [see *Hudson et al.*, 1996b, 1997, *Hudson and Liu*, 1999].

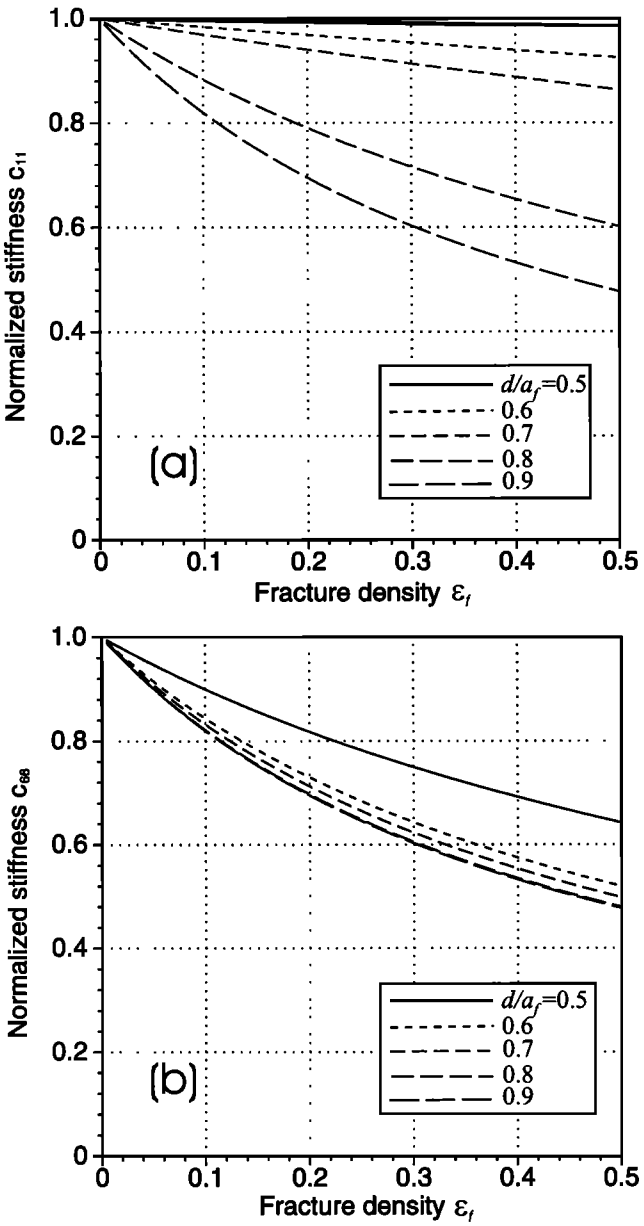

Figure 8. Variation of (a) normalized c_{11} and (b) c_{66} with fracture density ε_f computed for various values of the parameter d/a_f; d is the aperture (thickness) of the fracture (model 3) and a_f is the fracture length. Note that the fractures are filled with a weak solid with α_f = 1500 m/s, μ_f = 200 m/s, and ρ_f = 1.0 g/cm^3.

7. Discussion

In this paper we have introduced three types of fracture models that are basically simple physical representations of more complicated natural fracture surfaces. As in all effective medium theories of the type used here, the assumption is made that the results will be approximately the same as for a naturally occurring system of the same type (e.g., aligned fractures) if the values of the statistical parameters of the model are taken to be those of the more complex natural fracture system. The boundary conditions derived by *Hudson et al.* [1996b, 1997] for fracture surfaces with relatively small (model 1) and large (model 2) areas of slip have been used to compute effective elastic compliances of cracks and fractures in the framework of *Hill* [1963], *Schoenberg and Sayers* [1995], and *Sayers and Kachanov* [1995]. Both these two fracture models can be equivalently replaced by model 3 that is a continuous thin layer filled with a weak solid. Although we have assumed that our theory in model 1 is valid only for a small concentration of cracks, a comparison of the results that it produces with one claimed to be valid for large crack concentrations, i.e., the differential effective medium theory of *Nishizawa* [1982], indicates that our theory may be valid for crack density up to 0.5. However, for fractures with roughly equal areas of slip and welded contact, the case midway between those of models 1 and 2, the theory is more speculative. The formulae for model 2 are consistent with results from modeling the fracture surface as an array of spheres [*White*, 1983; see also *Hudson and Liu*, 1999], and the effective elastic constants for model 3 are in agreement with *Backus'* [1962] model. We suggest that the fracture models presented in this paper are general in the sense that many applications can be handled in a straightforward way. Some of these are discussed here.

Although (15) and (28) derived for the fracture compliance $\boldsymbol{s}^f$ under models 1 and 2, respectively, are of the same form, the parameters which appear in these expressions are different. For model 1 they are ε, the overall crack number density; ε_c, the number density of cracks on the fracture surface; and a_c/a_f, the ratio of crack size to fracture size. For model 2 they are ε_f, the fracture number density; ε_w, the number density of contacts on the fracture surface; and b/a_f, the ratio of contact size to fracture size. If we write r as the relative area of slip on the fracture surface, then

$$r = \pi\varepsilon_c = 1 - \pi\varepsilon_w. \tag{43}$$

Thus ε_c and ε_w are related, although model 1 is correct only for small ε_c (r small) and model 2 is correct only for small ε_w (r near 1). In the region around r = 0.5, there is no satisfactory theory. Extrapolation from both ends will give different results, depending on the values assigned to the parameters, and in any case neither model 1 nor model 2 is very convincing when there is equal area of slip and contact on a fracture.

For a given set of observations it is very likely that both models 1 and 2 will provide reasonable interpretations with appropriate values of the parameters; that is, we may expect that a small number of heavily cracked fractures will give the same result as a large number of lightly cracked fractures. Other information will be needed to come to the correct conclusions. As we have shown above, it is also possible to replace either model 1 or model 2 by model 3, although, once again, this may well be excluded on the basis of prior knowledge; e.g., the properties of the inferred material infilling the

fractures may not correspond to any material likely to be there.

The fracture models presented here are idealized in more than one aspects. Some of the restrictions we have placed on them can be relaxed in a fairly straightforward way. We consider two ways here of generalizing the models.

7.1. Nonaligned Fractures

The fractures on any fault are never completely aligned, and the effects of this nonalignment can be calculated by separating the fractures into sets, each set containing fractures of a given alignment. Multiple fracture sets can be added easily in the compliance domain as described by Schoenberg and his coauthors in several papers [e.g., *Schoenberg and Sayers*, 1995]. This is simply done by adding additional compliances of each fracture set using (12). When two fracture sets are combined, by definition the total fracture density $\varepsilon_{\text{total}}$ is simply the sum of fracture densities of each individual set denoted by ε_1 and ε_2

$$\varepsilon_{\text{total}} = \varepsilon_1 + \varepsilon_2, \tag{44}$$

and the average polarization ϕ_{average} of the fast split shear waves for near vertical propagation is approximately the fracture density weighted average of each individual fracture orientation (ϕ_1 and ϕ_2) and is given by

$$\phi_{\text{average}} \simeq \frac{\varepsilon_1\phi_1 + \varepsilon_2\phi_2}{\varepsilon_1 + \varepsilon_2}. \tag{45}$$

This means that in terms of shear wave propagation, multiple fracture sets may be effectively represented by a single set with the effective fracture density and fracture strike being replaced by (44) and (45), respectively. Equation (45) was first given by *Liu et al.* [1992] as an empirical expression, and it has been subsequently proven to be generally valid for a wide range of applications [*MacBeth*, 1996]. *MacBeth* [1996] and *Sayers* [1998] have also provided theoretical studies of the effects of multiple fracture sets.

7.2. Effects of Matrix Permeability and Porosity

The application of seismic anisotropy has been very successful in many geophysical applications [*Crampin*, 1994; *MacBeth*, 1995]. One of the main contributions has been its ability to estimate stress orientations and hence fluid flow anisotropy. Several studies have attempted to relate field measured seismic anisotropy to fluid flow in the rock-mass. *Queen and Rizer* [1990] show that seismic anisotropy can provide direct information about fracture orientations that are consistent with independent measurements and stress orientations. *Heffer et al.* [1995] and *Heffer and Koutsabeloulis* [1996] argue that fluid flow in many reservoirs is strongly dependent on stress. *Horne and MacBeth* [1996] have shown a strong correlation between shear wave anisotropy measured in vertical seismic profiles (VSPs) and permeability measured in cores. *Lynn et al.* [1996], *Lynn and Beckham* [1998], and *He and Zhang* [1996], in a series of papers, attempted to use seismic anisotropy to infer fluid flow direction and horizontal permeability anisotropy.

Hudson et al. [1996a] and Pointer et al. (submitted manuscript, 1999) have extended *Hudson*'s [1980, 1981] theory to allow fluid flow between cracks and fluid flow between cracks and porous rock, and the theory can be easily incorporated in the fracture models developed in this paper by replacing U_{11} and U_{33} in (14) with appropriate forms as explicitly given by Pointer et al. (submitted manuscript, 1999).

There have been several other theoretical studies aimed at relating permeability and/or porosity to the properties of seismic waves, and here we just mention a few. *Thomsen* [1995] studied the effects of matrix (equant) porosity on seismic anisotropy. Recently, *Zatsepin and Crampin* [1997] and *Crampin and Zatsepin* [1997] have developed an anisotropic poroelastic model, which predicts stress-dependent velocity and permeability anisotropy. *Xu* [1998] has also developed theory to model porous media containing a combination of pores of various aspect ratios (cracks and pores). He has also applied his theory to model the laboratory results of *Rathore et al.* [1995]. Mention must also be made of the squirt flow model [*Dvorkin and Nur*, 1993] and the Biot flow model [*Gelinsky and Shapiro*, 1995]. It is suggested that attenuation anisotropy may also be used to infer fluid flow anisotropy [*Pointer et al.*, 1996; *Lynn and Beckham*, 1998].

7.3. Fluid Content of Fractures

An indicator of fluid content in fractures proposed by *Schoenberg* [1998] is the normal to shear compliance ratio (Z_N/Z_T). For example, if fractures are dry, then $Z_N/Z_T \simeq 1$, and if fractures are filled with liquid, $Z_N/Z_T \simeq 0$. In general, if the fracture is filled with a fluid (assuming $\lambda_f \neq 0, \mu_f = 0$ and $\eta_f = 0$) and, for simplicity, if we assume the matrix rock is a Poisson medium (i.e., $\lambda = \mu$), we have for model 1 (from equation (14)),

$$\frac{Z_N}{Z_T} \simeq \frac{A'_N}{A'_T} = \frac{7}{8}\left[1 + \frac{9}{2\pi}\left(\frac{a_c}{c_c}\right)\left(\frac{\lambda_f}{\lambda + 2\mu}\right)\right]^{-1}, \tag{46}$$

where we have used the expressions for U_{11} and U_{33} for cracks filled with a weak material as given by *Hudson* [1981]; a_c and c_c are the long and short axes of the elemental cracks on the fracture planes (c_c/a_c is called the aspect ratio). Similarly, for model 3 we have (from equation (42a))

$$\frac{Z_N}{Z_T} \simeq \frac{C''_N}{C''_T} = \frac{7}{8}\left[1 + \frac{6}{\pi}\left(\frac{a_f}{d}\right)\left(\frac{\lambda_f}{\lambda + 2\mu}\right)\right]^{-1}. \tag{47}$$

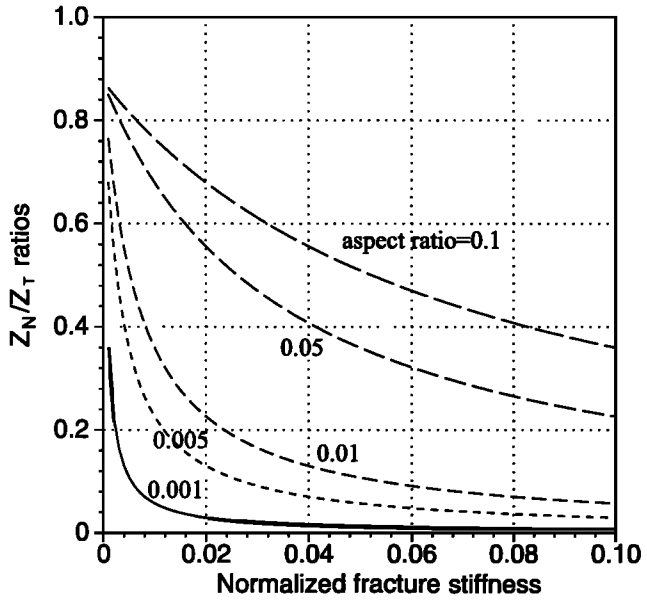

Figure 9. Variations of Z_N/Z_T ratios with normalized bulk modulus of the fracture infill $(\lambda_f/(\lambda + 2\mu))$ for different aspect ratios of element cracks as indicated on the curves (computed using equation (46) for model 1). The matrix is a Poisson's solid ($\lambda = \mu$).

Figures 9 and 10 show the variations of the fracture compliance ratio (Z_N/Z_T) with normalized bulk modulus of the fracture infill $(\lambda_f/(\lambda + 2\mu))$. The variations were computed for different crack aspect ratios (c_c/a_c) for model 1 (Figure 9) and different ratios of d/a_f for model 3 (Figure 10). Both Figures 9 and 10 show that Z_N/Z_T decreases as bulk modulus of the fracture infill increases with the rapid change occurring when the fracture infill bulk modulus approaches zero (i.e., gas-filled fractures). This shows the sensitivity of Z_N/Z_T to the fracture infill.

We mentioned earlier that the theory formulated for model 2 does not allow for the cracked regions to be filled with any material other than air (dry cracks) or an inviscid incompressible fluid. *Hudson and Liu* [1999] have shown that it is plausible to extend model 2 such that the region outside the welded contacts filled with material with arbitrary bulk and shear moduli κ_f $(= \lambda_f + (2/3)\mu_f)$, μ_f. A model fracture of this kind is equivalent to a model 3 fracture with a layer of thickness rd_w and elastic constants

$$\mu^* = \mu_f + \frac{8d_w\mu}{\pi b}\left(\frac{\lambda+\mu}{3\lambda+4\mu}\right) R, \tag{48a}$$

$$\kappa^* = \kappa_f - \frac{4d_w\mu}{3\pi b}\frac{(\lambda+\mu)(4\mu-\lambda)}{(3\lambda+4\mu)(\lambda+2\mu)} R, \tag{48b}$$

where we have written

$$R = r(1-r)\left[1+2\left(\frac{1-r}{\pi}\right)^{\frac{1}{2}}\right].$$

In the above equations $r = 1-\gamma_w\pi b^2$ and d_w is the mean aperture (thickness) of the region outside the contacts. It is essential for the validity of the theory that d_w/b be small. Put (48) into (34) and (35) and assume that the matrix is a Poisson solid (i.e., $\lambda = \mu$), and we have

$$\frac{Z_N}{Z_T} = \frac{16}{21\pi}R\left(\frac{d_w}{b}\right)\left[\frac{\lambda_f}{\lambda+2\mu} + \frac{8}{9\pi}R\left(\frac{d_w}{b}\right)\right]^{-1}, \tag{49}$$

We expect $\gamma_w\pi b^2$ to be small, say $0 \le \gamma_w\pi b^2 \le 0.5$ and therefore $0.5 \le r \le 1$, so we have $0 \le R \le 0.45$. Figure 11 shows the variation of the fracture compliance ratio (Z_N/Z_T) with normalized bulk modulus of fracture infill $(\lambda_f/(\lambda + 2\mu))$. The variations were computed using (49) for different ratios of d_w/b (assuming $R = 0.3$) as indicated in the figure, and the results show similar variations as for models 1 and 3 (Figures 9 and 10) with the rapid change occurring when the fracture infill bulk modulus approaches zero (i.e., gas-filled fractures). However, the decrease in Z_N/Z_T as the infill stiffness increases for model 2 (Figure 11) is much more dramatic than for models 1 and 3. Figure 11 together with Figures 9 and 10 indicate that the ratios of Z_N/Z_T are very sensitive to the properties of the fracture infill and can be effectively used as a measure of fluid content in fractures.

7.4. Scale Length, Fracture Criticality, and Limitation of Effective Medium Theories

Although estimates of fracture density and orientation of microcracks can be found from equivalent medium theories as studied in this paper, the appli-

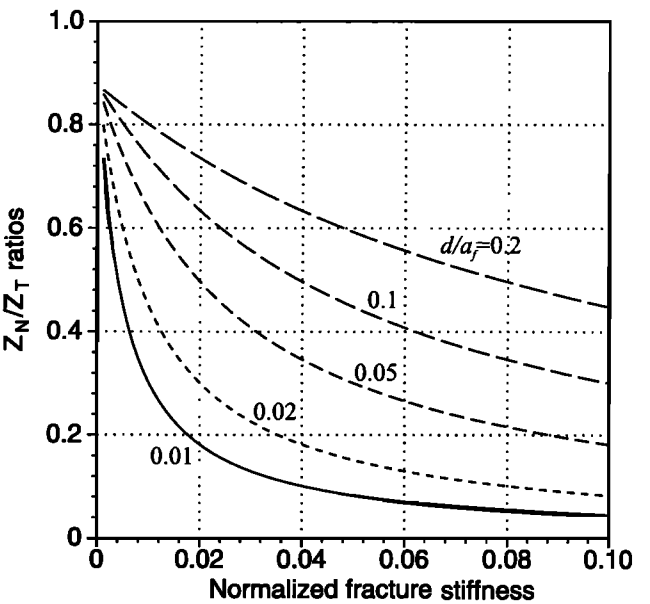

Figure 10. Variations of Z_N/Z_T ratios with normalized bulk modulus of the fracture infill $(\lambda_f/(\lambda+2\mu))$ for different ratios of d/a_f as indicated on the curves (computed using equation (47) for model 3). The matrix is a Poisson's solid ($\lambda = \mu$).

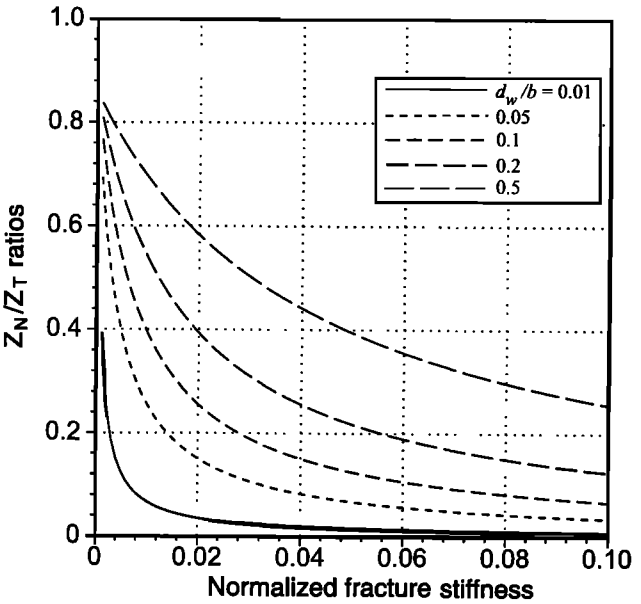

Figure 11. Variations of Z_N/Z_T ratios with normalized bulk modulus of the fracture infill ($\lambda_f/(\lambda+2\mu)$) for different ratios of d_w/b as indicated on the curves (computed using equation (49) for model 2). The matrix is a Poisson's solid ($\lambda = \mu$).

cation to seismic anisotropy is limited by the necessary theoretical constraints of dilute concentrations and very small scale size to wavelength ratios. This limitation has not yet been satisfactorily addressed in the use of seismic anisotropy for fracture characterization. It is believed that to some degree, natural fracture systems may not be consistent with conventional equivalent medium theory. They do not appear as dilute, randomly spaced, disconnected ideal shapes, nor are they weak scatterers. In contrast, they appear with spatial clustering and a distribution of scale lengths and regularity. They possess a degree of connectivity between different scales and discontinuous clustering or fragmentation reflecting past historical conditions, local geological weakness, and composite lithology [e.g., *Barton*, 1995]. These restrictions should be borne in mind when applying the above theories and considering future extensions to this work. Model 1 is valid for small crack density ($\varepsilon \ll 1$ and $\varepsilon_c \ll 1$), and model 2 is valid for small density of welded contacts ($\varepsilon_f \ll 1$ and $\varepsilon_w \ll 1$). As for model 3 (a thin layer filled with a weak material), it is valid for small porosity of fractures ($\varepsilon_f \ll 1$ and $\phi \ll 1$), and the assumption of noninteracting fracture systems in the formulae of *Sayers and Kachanov* [1995] and *Schoenberg and Sayers* [1995] once again implies that multiples between fracture planes are not considered. The weak assumption is generally believed to hold for crack densities up to about 0.1 [*Crampin*, 1984]. This is critical to all dilute concentration theories and is related to the onset of significant multiple scattering.

One of the criticisms of *Hudson*'s [1980, 1981] second-order theory is that it is "unphysical" for large crack density because elastic stiffness increases rather than decreases with an increase in crack density (solid lines in Figure 4) [*Cheng, 1993*, *Sayers and Kachanov*, 1995]. This unphysical behavior disappears in the theory as presented in this paper, and we show by comparison with the DEM of *Nishizawa* [1982], which is claimed to be valid for any crack density, that the theory developed in this paper based on Hudson's model is equally plausible at high-order crack density. The question is, do we need a theory which allows crack density larger than 0.1? If the concept of fracture criticality [*Crampin*, 1994] holds within the crust, the occurrence of multiple scattering at the microstructural level is limited.

If we do need to allow for high crack densities, then numerical experiments can be used to test whether a plausible theory fits the model it is based on. (Whether or not it is applicable to crustal rocks is another question which can only be answered by observations.) *Davis and Knopoff* [1995] used a two-dimensional (2-D) static boundary element method to study the effective response of randomly distributed cracks under antiplane strain and showed that the single scattering or first-order approximation provided accurate results even in a strongly interacting regime; i.e., for crack density $\gamma\pi a^2$ up to 2, where γ is the number of cracks per unit area and a is the mean half length of the cracks. However, a similar study by *Dahm and Becker* [1998] for cracks under in-plane strain suggests that crack-crack interactions cannot be simply ignored for high crack densities. Liu et al. (submitted to *Geophysical Journal International*, 1999) have used a 2-D dynamic boundary element method to simulate wave propagation in media with spatially distributed cracks. Scale length distributions (such as power law or fractal) can be easily considered with numerical methods, and it has been demonstrated that both spatial and scale length distributions have significant effects on wave fields. Numerical methods such as the boundary element method have the advantage that there is no restriction in the ratio of crack size to wavelength, and multiple crack-crack interactions between fractures can easily be handled without additional difficulty; they can be used to tackle a range of problems, such as to study short-wavelength scattering and to investigate the effects of fracture spacing, spatial distributions, scale length distributions, etc., on seismic wave fields. Its main drawback, however, is computing cost.

8. Conclusions

We have presented analytic expressions for the fracture compliance $\boldsymbol{Z}$ for three styles of fracture surface conditions. These fracture compliances may be regarded as macroscopic parameters to be determined by experiments. The main contribution of this paper is that given enough a priori information to select the more appropriate model for the fracture surfaces, it is then possible to infer some statistical details of its microstructure. From (25), (33) and (42) we find that for

all three fracture models the assumption of $Z_N/Z_T \simeq 1$ generally holds for dry fractures as Poisson's ratio ν is small (in the range $0.1 \leq \nu \leq 0.25$); the resultant fractured medium is called a scalar-fracture system by *Schoenberg and Sayers* [1995]. However, for liquid-filled fractures, $Z_N/Z_T \simeq 0$. So the Z_N/Z_T ratio can therefore be used as an effective indicator of fluid content in fractures. It is noted, however, that we have not considered stress-dependent fracture compliances [*Hillis*, 1998], and this is a subject of future studies. Our main results are summarized as follows:

1. A wide range of fractures can be modeled in one of the three ways: (1) a plane distribution of small cracks; (2) as a plane distribution of small isolated contacts; or (3) as thin layer with a weak infill.

2. Using the models, it is possible to relate the fracture compliance $\boldsymbol{Z}$ to details of the microscopic structure of the fracture surface. Thus, given enough a priori information to choose the correct model, it is possible to obtain the microstructural properties of fractured rock from measured seismic properties. In particular, the Z_N/Z_T ratio may be used as an indicator of fluid content in fractures.

3. Using the concept of average stress and strain and the linear slip assumption, most theories can be cast in a unified form and, to first-order in crack density, theories, such as those of *Schoenberg and Sayers* [1995], *Sayers and Kachanov* [1995], *White* [1982], and *Backus* [1962], can be shown to be consistent.

4. First-order theories contain information on first-order statistics only of the crack distribution; i.e., the number density of cracks. If information on second-order statistics (e.g., the extent of clustering of cracks) is required, second-order terms must be included in the theory.

5. Our results show that although all boundary conditions were derived for dilute concentrations of cracks (model 1) and contacts (model 2), plausible values at high crack concentrations are given. However, the notion of fracture criticality [*Crampin*, 1994] should be borne in mind when interpretation of field data is made.

Appendix A: Response of a Single Fracture to an Imposed Stress Field

On each of models 1, 2, and 3 of a fracture the conditions on the fracture surface (averaged over the microstructure in models 1 and 2) are

$$[u_1] = \zeta_N t_1, \quad [u_2] = \zeta_T t_2, \quad [u_3] = \zeta_T t_3, \tag{A1}$$

where $[\boldsymbol{u}]$ is the discontinuity in displacement across the fracture, which is oriented with normal in the one-direction, and $\boldsymbol{t}$ is the traction on the face of the fracture. We now wish to calculate the average displacement discontinuity over an isolated fracture lying in an unbounded matrix due to a uniform stress field $\boldsymbol{\sigma}$ imposed at infinity.

In the usual way we approximate the fracture by a spheroid of small aspect ratio c_f/a_f, where c_f is the semiminor axis and a_f is the semimajor axis of the spheroid. Under a homogeneous imposed stress field the strain within a homogeneous spheroidal inclusion is uniform [*Eshelby*, 1957], which means that

$$[\boldsymbol{u}] \propto (1 - r^2/a_f^2)^{1/2}, \tag{A2}$$

where r is the distance from the axis of the spheroid and $[\boldsymbol{u}]$ is the difference in displacements at equivalent points on the upper and lower faces of the ellipsoid. In order to accommodate this with a fracture condition such as (A1), we need to assume that ζ_N and ζ_T vary with r according to

$$\zeta_N = \frac{3}{2} Z_N (1 - r^2/a_f^2)^{1/2}, \tag{A3a}$$

$$\zeta_T = \frac{3}{2} Z_T (1 - r^2/a_f^2)^{1/2}, \tag{A3b}$$

where Z_N and Z_T are the mean values of ζ_N and ζ_T, respectively, over the fracture so that (3) holds.

If the faces of the ellipsoid were stress free, the imposition of a stress field $\boldsymbol{\sigma}^0$ would result in discontinuities in displacement given by [*Hudson*, 1980]

$$[u_1] = \sigma_{11}^0 \frac{2a_f}{\pi\mu}\left(\frac{\lambda + 2\mu}{\lambda + \mu}\right)(1 - r^2/a_f^2)^{1/2},$$

$$[u_2] = \sigma_{12}^0 \frac{8a_f}{\pi\mu}\left(\frac{\lambda + 2\mu}{3\lambda + 4\mu}\right)(1 - r^2/a_f^2)^{1/2}, \tag{A4}$$

$$[u_3] = \sigma_{13}^0 \frac{8a_f}{\pi\mu}\left(\frac{\lambda + 2\mu}{3\lambda + 4\mu}\right)(1 - r^2/a_f^2)^{1/2}.$$

We now superimpose a uniform stress and strain field corresponding to homogeneous matrix material and with

$$\sigma_{11} = \sigma_{11}^1 = \frac{4\sigma_{11}^0 a_f}{3\pi\mu Z_N}\left(\frac{\lambda + 2\mu}{\lambda + \mu}\right),$$

$$\sigma_{12} = \sigma_{12}^1 = \frac{16\sigma_{12}^0 a_f}{3\pi\mu Z_T}\left(\frac{\lambda + 2\mu}{3\lambda + 4\mu}\right), \tag{A5}$$

$$\sigma_{13} = \sigma_{13}^1 = \frac{16\sigma_{13}^0 a_f}{3\pi\mu Z_T}\left(\frac{\lambda + 2\mu}{3\lambda + 4\mu}\right).$$

This superimposed field does not significantly change the displacement discontinuity on the fracture since the aspect ratio is small. So, with the combined stress field $\boldsymbol{\sigma}^0 + \boldsymbol{\sigma}^1$ we have the displacement discontinuities given by (A4) and tractions on the fracture surface given by

$$t_j = \sigma_{1j}^1, \qquad j = 1, 2, 3.$$

As a result, (A1) are satisfied on the fracture surface.

The relevant components of the combined stress field at infinity are

$$\sigma_{11} = \sigma_{11}^0 + \sigma_{11}^1 = \sigma_{11}^0\Big[1 + \frac{4a_f}{3\pi\mu Z_N}\Big(\frac{\lambda+2\mu}{\lambda+\mu}\Big)\Big],$$

$$\sigma_{12} = \sigma_{12}^0 + \sigma_{12}^1 = \sigma_{12}^0\Big[1 + \frac{16a_f}{3\pi\mu Z_T}\Big(\frac{\lambda+2\mu}{3\lambda+4\mu}\Big)\Big], \quad \text{(A6)}$$

$$\sigma_{13} = \sigma_{13}^0 + \sigma_{13}^1 = \sigma_{13}^0\Big[1 + \frac{16a_f}{3\pi\mu Z_T}\Big(\frac{\lambda+2\mu}{3\lambda+4\mu}\Big)\Big],$$

and the integrated displacement discontinuities are

$$\begin{aligned}\int_S [u_1]dS &= \sigma_{11} S \frac{4a_f}{3\pi\mu}\Big(\frac{\lambda+2\mu}{\lambda+\mu}\Big) \\ &\quad \Big[1 + \frac{4a_f}{3\pi\mu Z_N}\Big(\frac{\lambda+2\mu}{\lambda+\mu}\Big)\Big]^{-1},\end{aligned}$$

$$\begin{aligned}\int_S [u_2]dS &= \sigma_{12} S \frac{16a_f}{3\pi\mu}\Big(\frac{\lambda+2\mu}{3\lambda+4\mu}\Big) \\ &\quad \Big[1 + \frac{16a_f}{3\pi\mu Z_T}\Big(\frac{\lambda+2\mu}{3\lambda+4\mu}\Big)\Big]^{-1}, \quad \text{(A7)}\end{aligned}$$

$$\begin{aligned}\int_S [u_3]dS &= \sigma_{13} S \frac{16a_f}{3\pi\mu}\Big(\frac{\lambda+2\mu}{3\lambda+4\mu}\Big) \\ &\quad \Big[1 + \frac{16a_f}{3\pi\mu Z_T}\Big(\frac{\lambda+2\mu}{3\lambda+4\mu}\Big)\Big]^{-1},\end{aligned}$$

where S is the area of the fault.

Alternatively, we may write the averaged displacement discontinuity $[\boldsymbol{u}]$ on the fracture as

$$\frac{1}{S}\int_S [u_1]\, dS = [\overline{u}_1] = T_N Z_N \sigma_{11},$$

$$\frac{1}{S}\int_S [u_2]\, dS = [\overline{u}_2] = T_T Z_T \sigma_{12}, \quad \text{(A8)}$$

$$\frac{1}{S}\int_S [u_3]\, dS = [\overline{u}_3] = T_T Z_T \sigma_{13},$$

where

$$T_N = \Big[1 + \frac{3\pi\mu Z_N}{4a_f}\Big(\frac{\lambda+\mu}{\lambda+2\mu}\Big)\Big]^{-1}, \quad \text{(A9a)}$$

and

$$T_T = \Big[1 + \frac{3\pi\mu Z_T}{16a_f}\Big(\frac{3\lambda+4\mu}{\lambda+2\mu}\Big)\Big]^{-1}. \quad \text{(A9b)}$$

This is the same as saying the traction $\boldsymbol{t}$ on the fault is given by

$$t_1 = T_N\sigma_{11}, \quad t_2 = T_T\sigma_{12}, \quad t_3 = T_T\sigma_{13}. \quad \text{(A10)}$$

Appendix B: Boundary Conditions for a Thin Layer With a Weak Solid Infill

Fehler [1982] studied the reflection and transmission response of a viscous fluid layer. Recently, *Groenenboom et al.* [1995], *Groenenboom and Fokkema* [1998], and *Rokhlin and Wang* [1991] have derived boundary conditions for a fracture modeled as a thin layer. They also studied the reflection and transmission properties of seismic waves across such fractures. However, all their derivations are very complicated. Here we give an alternative, but much simpler, derivation.

If the ratio of fracture thickness d to the wavelength of a seismic wave is very small (model 3, Figure 3c), then we may approximate the conditions on the fracture by taking the stress components σ_{i3}, where the three-component is normal to the fracture plane (i.e., $\boldsymbol{n} = (0, 0, 1)$), to be constant through the layer. Writing traction

$$t_i = \sigma_{i3}, \quad \text{(B1)}$$

we have

$$\begin{aligned}t_1 &= \Big(\mu_f + i\omega\eta_f\Big)\Big(\frac{\partial u_1}{\partial x_3} + \frac{\partial u_3}{\partial x_1}\Big) \\ &\simeq \Big(\mu_f + i\omega\eta_f\Big)\frac{\partial u_1}{\partial x_3}, \quad \text{(B2)}\end{aligned}$$

where μ_f is the rigidity and η_f is the viscosity of the material within the layer, since we expect quantities other than t_i to vary more rapidly through the weak layer than in other directions. It follows that

$$[u_1] = \frac{d}{\mu_f + i\omega\eta_f}t_1, \quad \text{(B3)}$$

(letting $\partial u_1/\partial x_3 = [u_1]/d$) and, similarly,

$$[u_2] = \frac{d}{\mu_f + i\omega\eta_f}t_2. \quad \text{(B4)}$$

Finally,

$$t_3 \simeq \Big(\lambda_f + 2\mu_f + \frac{4}{3}i\omega\eta_f\Big)\frac{\partial u_3}{\partial x_3}, \quad \text{(B5)}$$

where λ_f is the second Lamé constant of the material infill, and so

$$[u_3] = \frac{d}{\lambda_f + 2\mu_f + \frac{4}{3}i\omega\eta_f}t_3. \quad \text{(B6)}$$

Equations (B3), (B4), and (B6) show that the shear compliance is

$$Z_T = \frac{d}{\mu_f + i\omega\eta_f} = \frac{d}{\mu}C_T, \quad \text{(B7)}$$

and the normal compliance is

$$Z_N = \frac{d}{\lambda_f + 2\mu_f + \frac{4}{3}i\omega\eta_f} = \frac{d}{\mu}C_N, \tag{B8}$$

where C_T and C_N are given as

$$C_T = \frac{\mu}{\mu_f + i\omega\eta_f}, \tag{B9a}$$

$$C_N = \frac{\mu}{\lambda_f + 2\mu_f + \frac{4}{3}i\omega\eta_f}. \tag{B9b}$$

These results are the generalisation of the boundary conditions given by *Murty* [1976] and *Yanovskaya and Dimtriyeva* [1991].

In order to test the accuracy of (B7) and (B8) in approximating a thin layer we have compared the reflection/transmission coefficients calculated using exact solutions with those using the above boundary conditions. The exact solutions were given by *Fehler* [1982] (with several typographic errors corrected), and the reflection and transmission coefficients for the slip boundary conditions were calculated using the equations given by *Pyrak-Nolte et al.* [1990]. The results were given in our earlier paper [*Liu et al.*, 1995], where a very good agreement was shown between the slip boundary conditions and the exact solutions obtained by *Fehler* [1982].

Notation

ϵ_{ij} components of strain.
σ_{ij} components of stress.
$[u_i]$ displacement jump (discontinuity) on fracture.
$[\overline{u}_i]$ mean jump in displacement on fracture.
$\boldsymbol{t}$, t_i traction tensor on a fracture.
$\boldsymbol{n}$, n_i normal to fracture surface.
λ, μ Lamé constants of unfractured rock.
ρ density of unfractured rock.
ν Poisson's ratio of unfractured rock, equal to $\lambda/[2(\lambda+\mu)]$.
α, β P and S wave velocities in unfractured rock.
$\boldsymbol{s}$, s_{ijkl} compliance tensor of fractured rock (inverse of stiffness tensor).
$\boldsymbol{s}^0$, s^0_{ijkl} compliance tensor of unfractured rock.
$\boldsymbol{s}^f$, s^f_{ijkl} additional compliance tensor due to fractures.
$\boldsymbol{Z}$, Z_{ij} fracture compliance tensor (from definition $[\overline{u}_i] = Z_{ij}t_j$).
Z_N, Z_T normal and transverse compliances of a fracture.
δ_{ij} Kroneker delta; $\delta_{ij} = 0$ if $i \neq j$ and $\delta_{ij} = 1$ if $i = j$.
T_{ij} tensor relating traction $\boldsymbol{t}$ on the fracture to the imposed stress $\boldsymbol{\sigma}$.
T_N, T_T diagonal values of the tensor $\{T_{ij}\}$ orientated with the fracture.
Z'_N, Z'_T $Z'_N = Z_N T_N$ and $Z'_T = Z_T T_T$.
V total volume of fractured region.
S mean area of fracture.
N_f number of fractures within V.
N_c mean number of cracks on a fracture (model 1).
γ_c number of cracks per unit area of fracture, equal to N_c/S (model 1).
D_f number of fractures per unit length, equal to $N_f S/V = H_f^{-1} = l_c^2/l^3 = \varepsilon/(a_c\varepsilon_c)$.
H_f mean spacing between fractures, equal to D_f^{-1}.
a_f mean fracture radius.
a_c mean crack radius (model 1).
c_c/a_c aspect ratio of cracks (model 1).
N total number of small cracks, equal to $N_f Nc$ (model 1).
ε overall number density of cracks (model 1), equal to Na_c^3/V.
ε_c number density of cracks on a fracture (model 1), equal to $\gamma_c a_c^2$.
ε_f number density of fractures, equal to $N_f a_f^3/V$.
A_N, A_T see equations (14a) and (14b) (model 1).
A'_N, A'_T see equations (16a) and (16b) (model 1).
l overall mean spacing between cracks ($l^3 = V/N$) (model 1).
l_c mean distance between cracks on a fracture ($l_c^2 = S/N = \gamma_c^{-1}$) (model 1).
U_{11}, U_{33} response of a single crack to shear and tension.
U^d_{11}, U^d_{33} response of a single dry crack to shear and tension.
E_N, E_T see equation (19).
c_{ij} elements of elastic stiffness matrix for fractured rock in the Voigt (6x6) notation (inverse of elastic compliance).
B_N, B_T see equations (27a) and (27b) (model 2).
B'_N, B'_T see equations (29a) and (27b) (model 2).
N_w number of contacts on a fracture (model 2).
γ_w number of contacts per unit area of fracture, equal to N_w/S (model 2).
b mean radius of contact (welded) regions (model 2).
ε_w number density of contacts on a fracture (model 2), equal to $\gamma_w b^2$.
d_w mean aperture of slip region (model 2).
r relative area of slip on a fracture, equal to $\gamma_c \pi a_c^2$ for model 1 and $1 - \gamma_w \pi b^2$ for model 2.
λ_f, μ_f Lamé constants of fracture infill.
η_f viscosity of fracture infill.
α_f, β_f P and S wave velocities of fracture infill.
ρ_f density of fractured infill.
d mean fracture aperture (model 3).
C_N, C_T see equations (35a) and (35b) (model 3).
C'_N, C'_T see equations (37a) and (37b) (model 3).
C''_N, C''_T see equations (39a) and (39b) (model 3).
ϕ porosity of fractured material (or called fracture porosity, equal to $dD_f = N_f S d/V$) (model 3).

ε_1, ε_2 number density of fractures in differently orientated fracture sets.

Acknowledgments. We thank our colleagues David Booth, Steve Horne (now at Schlumberger Cambridge Research), Xiang Yang Li, and Frank Ohlsen for their comments on this work. We are particularly indebted to John Queen (Conoco Inc.) and Bill Rizer (formerly with Conoco Inc.) for many invaluable discussions and for their guidance during the course of this research. We also thank JGR reviewers (Larry Myer and Feng Shen) and Associate Editor (Richard Carlson) for their constructive comments. The first author (E.L.) would also like to thank Joeren Groenenboom of Delft University of Technology, Zeng Xinwu and Zhang Zhongjie of the Chinese Academy of Sciences, Larry Myer and Kurt Nihei of Lawrence Berkeley Laboratory, Shen Feng of MIT, Xu Shiyu of Mobil, and Julio Setsuo of Petrobras for useful discussions about fractures and fracture boundary conditions. This work was supported by a NERC micro-to-Macro ($\mu 2M$) project. This paper is published with the approval of the Director of the British Geological Survey (NERC).

References

Angel, Y. C., and J. D. Achenbach, Reflection and transmission of elastic waves by a periodical array of cracks, *J. Appl. Mech., 52*, 33-41, 1985.

Auld, B. A., *Acoustic Fields and Waves in Solids*, 2nd ed., Krieger, Melbourne, Fla., 1990.

Backus, G. E., Long-wave elastic anisotropy produced by horizontal layering, *J. Geophys. Res., 67*, 4427-4440, 1962.

Barton, C. C., Fractal analysis of scaling and spatial clustering of fractures, in *Fractals in the Earth Sciences*, edited by C.C. Barton and P.R. LaPointe, pp.121-134, Plenum, New York, 1995.

Batzle, M., and Z. Wang, Seismic properties of pore fluids, *Geophysics, 57*, 1396-1408, 1992.

Cheng, C. H., Crack models for a transversely isotropic medium, *J. Geophys. Res., 98*, 675-684, 1993.

Cosgrove, J. W., The role of structural geology in reservoir characterization, in *Structural Geology in Reservoir Characterization*, edited by M. P. Coward, T. S. Daltaban, and H. Johnson, *Geol. Soc. Spec. Publ., 127*, 1-13, 1998.

Crampin, S., Effective elastic constants of wave propagation in cracked media, *Geophys. J. R. Astron. Soc., 76*, 135-145, 1984.

Crampin, S., The fracture criticality of crustal rock, *Geophys. J. Int., 118*, 428-438, 1994.

Crampin, S., and B. K. Atkinson, Microcracks in the Earth's crust, *First Break, 3*, 16-20, 1985.

Crampin, S., and S. V. Zatsepin, Modeling the compliance of crustal rock, II, Response to temporal changes before earthquakes, *Geophys. J. Int., 129*, 495-506, 1997.

Dahm, T., and T. H. Becker, On the elastic and viscous properties of media containing strongly interacting in-plane cracks, *Pure Appl. Geophys., 151*, 1-16, 1998.

Davis, P. M., and L. Knopoff, The elastic modulus of media containing strongly interacting antiplane cracks, *J. Geophys. Res., 100*, 18,253-18,258, 1995.

Dvorkin, J., and A. Nur, Dynamic poroelasticity: A unified model with the squirt and the Biot mechanisms, *Geophysics, 58*, 524-533, 1993.

Eshelby, J. D., The determination of the elastic field of an ellipsoidal inclusion, and related problems, *Proc. R. Soc. London Ser. A 241*, 376-396, 1957.

Fehler, M., Interaction of seismic waves with a viscous liquid layer, *Bull. Seismol. Soc. Am., 72*, 55-72, 1982.

Gangi, A. F., The variation of mechanical and transport properties of cracked rock with pressure, *Proc. U.S. Symp. Rock Mech., 22nd*, 85-89, 1981.

Gelinsky, S., and S. A. Shapiro, Anisotropic permeability: influence on seismic velocity and attenuation, paper presented at 6th International Workshop on Seismic Anisotropy, Soc. of Explor. Geophys., Trondheim, Norway, 1995.

Groenenboom, J., and J. T. Fokkema, Monitoring the width of hydraulic fractures with acoustic waves, *Geophysics, 63*, 139-148, 1998.

Groenenboom, J., A. J. W. Duijndam, and J. T. Fokkema, Hydraulic fracture characterization with dispersion measurements of seismic waves, paper presented at 65th Annual International SEG Meeting, Soc. of Explor. Geophys., Los Angels, Cal., 926-929, 1995.

He, Q. D., and Z. J. Zhang, *Wave Propagation in Cracked Media: Excitation and Numerical Modelling* (in Chinese), Jilin Univ. Press, Changchun, China, 1996.

Heffer, K., R. J. Fox, C. A. McGill, and N. C. Koutsabeloulis, Novel techniques show links between reservoir flow directionality, Earth stress, fault structure, and geometrical changes in mature water floods, SPE paper 30711 presented at SPE Annual Technical Conference, Soc. of Pet. Eng., Houston, Tex., 1995.

Heffer, K., and N. C. Koutsabeloulis, The dynamic 3-D reservoir - both hydraulically and geometrically, SPE paper 35519 presented at NFP/SPE European 3-D Reservoir Modeling Conference, Soc. of Pet. Eng., Stavanger, Norway, 1996.

Hill, R., Elastic properties of reinforced solids: Some theoretical principles, *J. Mech. Phys. Solids, 11*, 357-372, 1963.

Hillis, R. R., The influence of fracture stiffness and the in situ stress field on the closure of natural fractures, *Pet. Geosci., 4*, 57-65, 1998.

Horne, S., and C. MacBeth, Global optimization methods for near-offset VSP inversion, paper presented at SEG/EAGE Summer Research Workshop, Soc. of Explor. Geophys., Big Sky, Mont., 1996.

Hudson, J. A., Overall properties of a cracked solids, *Math. Proc. Cambridge Philos. Soc., 88*, 371-384, 1980.

Hudson, J. A., Wave speeds and attenuation of elastic waves in material containing cracks, *Geophys. J. R. Astron. Soc., 64*, 133-150, 1981.

Hudson, J. A, Seismic wave propagation through material containing partially saturated cracks, *Geophys. J., 92*, 33-37, 1988.

Hudson, J. A., and L. Knopoff, Predicting the overall properties of composite materials with small-scale inclusions or cracks, *Pure Appl. Geophys., 131*, 551-576, 1989.

Hudson, J. A., and E. Liu, Effective elastic properties of heavily faulted structures, *Geophysics, 64*, 479-485, 1999.

Hudson, J. A., E. Liu, and S. Crampin, The mechanical properties of materials with interconnected cracks and pores, *Geophys. J. Int., 124*, 105-112, 1996a.

Hudson, J. A., E. Liu, and S. Crampin, Transmission properties of a plane fault, *Geophys. J. Int., 125*, 559-566, 1996b.

Hudson, J. A., E. Liu, and S. Crampin, The mean transmission properties of a fault with imperfect facial contact *Geophys. J. Int., 129*, 720-726, 1997.

Jones, G. and R. J. Knipe, Seismic attribute maps: Application to structural interpretation and fault seal analysis in the North Sea basin, *First Break, 12*, 449-461, 1996.

Jones, J. P., and J. S. Whittier, Waves at a flexibly bonded interface-elastic layer, *J. Appl. Mech., 34*, 904-909, 1967.

Kozlov, E. A., Reflection of seismic waves from loaded (fracture) layers with nonwelded contacts, paper presented at

67th Annual International SEG Meeting, Soc. of Explor. Geophys., Dallas, Tex., 2009-2012, 1997.

Liu, E., S. Crampin, J. H. Queen, and W. D. Rizer, Behavior of shear waves in rocks with two sets of cracks, *Geophys. J. Int., 113*, 509-517, 1992.

Liu, E., J. H. Hudson, S. Crampin, W. D. Rizer, and J. H. Queen, Seismic properties of a general fracture, in *Mechanics of Jointed and Faulted Rock*, edited by H. P. Rossmanith, pp.673-678, A. A. Balkema, Brookfield, Vt., 1995.

Liu, E., C. MacBeth, T. Pointer, J. H. Hudson, and S. Crampin, The effective elastic compliance of fractured rock, paper presented at 66th Annual International SEG Meeting, Soc. of Explor. Geophys., Denver, Colo., 1882-1885, 1996.

Liu, E., S. Crampin, and J. A. Hudson, Diffraction of seismic waves by cracks with application to hydraulic fracturing, *Geophysics, 62*, 253-265, 1997.

Lynn, H., and W. Beckham, *P*-wave azimuthal variations in attenuation, amplitude, and velocity in 3-D field data: Implication for mapping horizontal permeability anisotropy, paper presented at 68th Annual International SEG Meeting, Soc. of Explor. Geophys., New Orleans, La., 193-196, 1998.

Lynn, H., K. M. Simon, C. R. Bates, and R. Van Dok, Naturally fractured gas reservoirs, seismic characterization, paper presented at 66th Annual International SEG Meeting, Soc. of Explor. Geophys., Denver, Colo., 1360-1363, 1996.

MacBeth, C., How can anisotropy be used for reservoir characterization?, *First Break, 13*, 31-37, 1995.

MacBeth, C., Interpreting qS_1 polarizations due to intersecting fractures, *Expanded Abstract, 66th Ann. Int. SEG Meeting*, 758-761, 1996.

Meadows, M., and D. W. Winterstein, Seismic detection of a hydraulic fracture from shear wave VSP data at Lost Hills field, *Geophysics, 59*, 11-26, 1994.

Murty, G. S., Reflection, transmission and attenuation of elastic waves at a loosely bonded interface of two half-spaces, *Geophys. J. R. Astron. Soc., 44*, 389-404, 1976.

Myer, L. R., L. J. Pyrak-Nolte, and N. G. W. Cook, Effects of single fractures on seismic wave propagation, in *Rock Joints*, edited by C. C. Barton and A. Stephenson, pp.1-12, A. A. Balkema, Brookfield, Vt., 1990.

Nagy, P. B., Ultrasonic classification of imperfect interfaces, *J. Nondestr. Eval., 11*, 127-139, 1992.

Newmark, N. M., C. P. Siess, and I. M. Viest, Tests and analysis of composite beams with incomplete interaction, *Proc. Soc. Esp. Stress Anal., 9*, 75-92, 1951.

Nihei, K. T., L. R. Myer, N. G. W. Cook, and W. Yi, Effects of nonwelded interfaces on guided SH-waves, *Geophys. Res. Lett., 21*, 745-748, 1994.

Nishizawa, O., Seismic velocity anisotropy in a medium containing oriented cracks: transversely isotropic case, *J. Phys. Earth, 30*, 331-347, 1982.

Nye, J. F., *Physical Properties of Crystals*, Oxford Univ. Press, New York, 1985.

Pointer, T., E. Liu, J. H. Hudson, and S. Crampin, Seismic wave propagation in media with interconnected cracks and pores, paper presented at 66th Annual International SEG Meeting, Soc. of Explor. Geophys., Denver, Colo., 1846-1849, 1996.

Pyrak-Nolte, L. J., L. R. Myer, and N. G. W. Cook, Transmission of seismic waves across single natural fractures, *J. Geophys. Res., 95*, 8617-8638, 1990.

Queen, J. H., and W. D. Rizer, An integrated study of seismic anisotropy and the natural fracture systems at the Conoco Borehole Test Facility, *J. Geophys. Res., 95*, 11255-11273, 1990.

Queen, J.H., W. D. Rizer, and D. DeMartini, Geophysical methods of fracture detection and estimation, *Leading Edge, 11*, 19-21, 1992.

Rathore, J., E. Fjaer, R. M. Holt, and L. Renlie, *P*- and *S*-wave anisotropy of a synthetic sandstone with controlled crack geometry, *Geophys. Prospect., 43*, 711-728, 1995.

Rokhlin, S. I., and Y. J. Wang, Analysis of boundary conditions for elastic wave interaction with an interface between two solids, *J. Acoust. Soc. Am., 89*, 503-515, 1991.

Sayers, C. M., Misalignment of the orientation of fractures and the principal axes for *P*- and *S*- waves in rocks containing multiple nonorthogonal fracture sets, *Geophys. J. Int., 133*, 459-469, 1998.

Sayers, C. M., and M. Kachanov, Microcrack-induced elastic wave anisotropy of brittle rocks, *J. Geophys. Res., 100*, 4149-4156, 1995.

Schoenberg, M., Elastic wave behavior across linear slip interfaces, *J. Acoust. Soc. Am., 68*, 1516-1521, 1980.

Schoenberg, M., Acoustic characterization of underground fractures, paper presented at 68th Annual International SEG Meeting, Soc. of Explor. Geophys., New Orleans, La., 1624-1627, 1998.

Schoenberg, M., and J. Douma, Elastic wave propagation in media with parallel fractures and aligned cracks, *Geophys. Prospect., 36*, 571-589, 1988.

Schoenberg, M., and F. Muir, A calculus for finely layered anisotropic media, *Geophysics, 54*, 581-589, 1989.

Schoenberg, M., and C. M. Sayers, Seismic anisotropy of fractured rock, *Geophysics, 60*, 204-211, 1995.

Stoll, R. D., Stress-induced anisotropy in sediment acoustics, *J. Acoust. Soc. Am., 85*, 702-708, 1989.

Thomsen, L., Elastic anisotropy due to aligned cracks in porous rock, *Geophys. Prospect., 43*, 805-829, 1995.

Tleukenov, S. K., Contact conditions of elastic media with an inter-layer, *J. Sov. Math, 55*, 1763-1766, 1991.

White, J. E., *Underground Sounding-Application of Seismic Waves*, Elsevier Sci., New York, 1983.

Xu, S., Modeling the effects of fluid communication on velocities in anisotropic porous rocks, *Int. J. Solids Struct., 35*, 4685-4707, 1998.

Xu, S., and M. S. King, Modeling the elastic and hydraulic properties of fractured rocks, *Mar. Pet. Geol., 9*, 155-166, 1992.

Yanovskaya, T. B., and L. A. Dimtriyeva, Effects of nonrigidity of the contact of elastic media on the coefficients of reflection, refraction and transfer, *Izv. Acad. Sci. USSR Phys. Solid Earth, Engl. Transl., 27*, 122-127, 1991.

Yoshioka, N., Elastic behavior of contacting surfaces under normal loads: a computer simulation using three-dimensional surface topographies, *J. Geophys. Res., 99*, 15,549-15,560, 1994.

Zatsepin, S. V., and S. Crampin, Modeling the compliance of crustal rock. I, Response of shear wave splitting to differential stress, *Geophys. J. Int., 129*, 477-479, 1997.

J.A. Hudson, Department of Applied Mathematics and Theoretical Physics, University of Cambridge, Silver Street, Cambridge CB3 9EW, England, UK. (J.A.Hudson@damtp.cam.ac.uk)

E. Liu, British Geological Survey, Murchison House, West Mains Road, Edinburgh EH9 3LA, Scotland, UK. (E.Liu@bgs.ac.uk)

T. Pointer, BG plc., Gas Research and Technology Centre, Ashby Road, Loughborough, Leicestershire LE11 3GR, England, UK. (timp@bgtech.co.uk)

(Received March 11, 1999; revised August 13, 1999; accepted August 25, 1999.)